Posttranslational modification of the RHO of plants protein RACB by phosphorylation and cross-kingdom conserved ubiquitination

Lukas Weiß[1], Tina Reiner[1], Julia Mergner[3], Bernhard Kuster[3,4], Attila Fehér[2], Götz Hensel[5], Manfred Gahrtz[5], Jochen Kumlehn[5], Stefan Engelhardt[1], Ralph Hückelhoven[1]*

*Corresponding author; mail: hueckelhoven@wzw.tum.de

Affiliations:

[1]Chair of Phytopathology, Technical University of Munich (TUM), Freising, Germany

[2]Chair of Plant Biology, University of Szeged, and Institute of Plant Biology, Biological Research Centre, Szeged, Hungary

[3]Chair of Proteomics and Bioanalytics, Technical University of Munich (TUM), Freising, Germany

[4]Bavarian Biomolecular Mass Spectrometry Center (BayBioMS), TUM, Freising, Germany

[5]Institute of Plant Genetics and Crop Plant Research (IPK), Gatersleben

Abstract

Small RHO-type G-proteins act as signaling hubs and master regulators of polarity in eukaryotic cells. Their activity is tightly controlled, as defective RHO signaling leads to aberrant growth and developmental defects. Two major pathways regulate G-protein activity: canonical switching of the nucleotide bound state and posttranslational modification (PTM). PTMs can support or suppress RHO signaling, depending on each individual case. In plants, regulation of Rho of plants (ROPs) has been shown to act through nucleotide exchange and hydrolysis, as well as through lipid modification, but there is little data available on phosphorylation or ubiquitination of ROPs. Hence, we applied proteomic analyses to identify PTMs of the barley ROP RACB. We observed *in vitro* phosphorylation by barley ROP Binding Kinase 1 and *in vivo* ubiquitination of RACB. Comparative analyses of the newly identified RACB phosphosites and

human RHO protein phosphosites revealed conservation of modified amino acid residues, but no overlap of actual phosphorylation patterns. However, the identified RACB ubiquitination site is present in all ROPs from *Hordeum vulgare*, *Arabidopsis thaliana* and *Oryza sativa*. Since this highly conserved amino acid residue is likewise ubiquitinated in mammalian Rac1 and Rac3, we suggest that RHO family proteins from different kingdoms could be generally regulated by ubiquitination of this site.

32 # Introduction

33 Small guanosine triphosphate-binding (G-) proteins are master regulators of developmental
34 and immunity-related processes. These include membrane transport, nuclear protein
35 trafficking, reactive oxygen species production and cytoskeleton organization in growth and
36 immunity (1-6). In humans (*Homo sapiens*, Hs), they are organized in the rat sarcoma (RAS)
37 superfamily, comprised of the ARF, RAB, RAN, RAS and RHO families (7), with the latter being
38 further divided into Cdc42-like, Rho-like, RAC-like, RhoBTB and Rnd subfamilies (8). Plants
39 however possess ARF, RAB and RAN family proteins, but only one type of small G-proteins
40 from the RAS homologue (RHO) family, so called Rho of plants (ROPs). Traditionally, they
41 were also called plant RACs (RAS-related C3 botulinum toxin substrate), due to their slightly
42 higher similarity to metazoan RACs than RHO proteins. ROPs can be further distinguished
43 based on their C-terminal hypervariable region and associated lipid modification. Type I ROPs
44 can be reversibly *S*-acylated and additionally contain a CaaX-box motif that is a target for
45 constitutive cysteine prenylation. Type II ROPs lack the CaaX-motif and are apparently
46 constitutively *S*-acylated. Those cysteine lipid modifications are essential for plasma
47 membrane anchoring and downstream signaling (9, 10). Additionally, RHO proteins are often
48 called molecular switches, as they cycle between a guanosine diphosphate (GDP)-bound
49 "OFF" state and guanosine triphosphate (GTP)-bound "ON" state. The nucleotide cycling itself
50 is tightly controlled by a set of specific proteins: guanosine nucleotide exchange factors (GEFs)
51 facilitate the GDP to GTP exchange, which leads to G-protein activation. In turn, GTPase
52 activating proteins (GAPs) target GTP-bound G-proteins and stimulate their weak intrinsic
53 GTPase activity to hydrolyse GTP to GDP to turn them "OFF" again (11). This nucleotide
54 exchange is accompanied by a conformational shift, which affects interaction with other
55 proteins (12, 13). A third class of regulatory proteins, so-called guanine nucleotide dissociation
56 inhibitors (GDIs), target mostly the GDP-bound state and recruit the G-protein to the cytoplasm,
57 blocking it from downstream signaling (14).

58 Lipidations are not the only posttranslational modifications (PTM) in RHO proteins. In animals
59 both phosphorylation and ubiquitination are employed to control RHO signaling, thereby
60 enhancing or suppressing G-protein function in a case-dependent manner. The mammalian
61 RHO family member Rac1 for instance is phosphorylated at three amino acids by different
62 kinases: focal adhesion kinase (FAK) and proto-oncogene tyrosine-protein kinase Src (cellular
63 sarcoma) phosphorylate Rac1 *in vitro* at Y64 (15). Phosphomimetic Rac1-Y64D mutants
64 showed decreased GTP-binding and association with downstream signaling proteins, and cells
65 expressing Rac1-Y64D displayed defects in focal adhesion targeting and cell spreading.
66 Extracellular signal-related kinase (ERK) phosphorylates Rac1 at T108, targeting it to the
67 nucleus before prenylation and hence isolating it from activation by cytosolic GEFs (16).
68 Phosphorylation of Rac1 by the AGC kinase AKT (RAC-alpha serine/threonine-protein kinase
69 1) at S71 has been shown to be essential for targeting by an F-box/Leucine-rich repeat (FBXL)
70 protein (17, 18). F-box proteins are part of SKP1-CUL1-F-box (SCF) E3 ubiquitin ligase
71 complexes which mediate ubiquitination and proteasomal degradation of selected proteins
72 (19). SCF^{FBXL19} targets S71-phosphorylated Rac1, which leads to ubiquitination of Rac1 K166
73 (18). This depletes Rac1 from cells, which inhibits its function in cell spreading. Another Rac1
74 ubiquitination site is K147, which is targeted by HECT domain and ankyrin repeat containing
75 E3 ubiquitin protein ligase 1 (HACE1) and two inhibitor of apoptosis proteins (IAPs). While
76 HACE1 mainly targeted GTP-bound Rac1, both XIAP and c-IAP1 did not show any preference
77 for a particular nucleotide-bound state. In all cases, ubiquitination of K147 leads to proteasomal
78 degradation of Rac1, abolishing its function in cell migration (20-22). For mammalian RhoA,
79 four phosphorylation sites and three ubiquitination sites have been identified. Phosphorylation
80 of S26 by mammalian Sterile20-related kinase 3 (Mst3) leads to increased intrinsic GTPase
81 activity of RhoA and associated depolymerization of F-actin, which is necessary for proper
82 neuron positioning in the developing mouse brain (23). ERK phosphorylates RhoA at S88 and
83 T100, enhancing GTP-binding and actin stress fiber formation in mammalian cell lines (24). In
84 contrast, protein kinase A (PKA)-mediated phosphorylation of S188 results in eviction of RhoA
85 from the plasma membrane with the help of RhoGDI, impeding RhoA function and protecting

86 it from ubiquitin-mediated degradation (25-28). Ubiquitination of RhoA has also been
87 demonstrated, with K6 and K7 being targets of Smad ubiquitylation regulatory factor 1
88 (Smurf1), while K135 is ubiquitinated by SCF^{FBXL19}. These modifications resulted in a loss of
89 tight junctions in epithelial cells and suppressed RhoA-mediated cytoskeleton organization and
90 cell proliferation, respectively (29, 30) (for an overview of Rac1 and RhoA PTMs, see S1 Fig).

91 Compared to the mammalian field, knowledge about phosphorylation and ubiquitination in
92 ROPs is limited. To date, phosphorylation of *Arabidopsis thaliana* (At) ROP4 and ROP6 by
93 ROP BINDING PROTEIN KINASE 1 (RBK1), a receptor-like cytoplasmic kinase (RLCK) of
94 class VI_A, has been shown. RBK1 interacts with Mitogen-activated protein kinase 1 (MPK1)
95 of an auxin-responsive MPK cascade, indicating that regulation of ROP4 and ROP6 via
96 phosphorylation might be important for auxin-dependent cell expansion (31). Furthermore,
97 type II AtROP10 and AtROP11 are phosphorylated at S138, but no functional studies about
98 these phosphosites have been conducted yet (32). Introduction of a phosphomimetic S-to-E
99 mutation of the broadly conserved S74 in AtROP4 and *Medicago sativa* MsROP6 has been
100 investigated. The S74E mutation did not alter GTPase activity, but blocked interaction with an
101 upstream activating ROPGEF, weakened binding to a downstream signaling kinase and
102 showed lesser *in vitro* kinase activation (33). However, evidence for *in vivo* phosphorylation of
103 type I ROPs is lacking.

104 In barley (*Hordeum vulgare, Hv*), ROPs have been investigated in the interaction between
105 barley and the powdery mildew fungus *Blumeria graminis* f.sp. *hordei* (*Bgh*). There, it was
106 shown that most barley ROPs are supporting the penetration success of *Bgh* (34-37). Among
107 these ROPs, RACB is the best characterized ROP family member. Under physiological
108 conditions, it is required for root hair outgrowth and stomatal subsidiary cell formation. RACB
109 and its interacting proteins further steer cytoskeleton organization (35, 38-40). During *Bgh*
110 attack, however, it was shown that RNA-interference (RNAi)-mediated knockdown of RACB
111 decreased the penetration success of the fungus into barley epidermal cells, whereas
112 overexpression of constitutively activated RACB (CA, RACB-G15V) promoted susceptibility

113 (34-37). In contrast, transient overexpression of neither wildtype (WT) nor dominant negative
114 RACB (DN, RACB-T20N) increased barley susceptibility, indicating that the GTP-bound, active
115 form of RACB supports fungal invasion into intact barley cells.

116 Since RHO family proteins interact with several downstream effectors in order to perform their
117 function in signaling, interaction partners of RACB were investigated with regard to barley
118 susceptibility to *Bgh*. It was shown that two classes of scaffolding proteins, ROP-interactive
119 partners (RIPs) and ROP-interactive and CRIB-domain containing proteins (RICs), associate
120 with CA-RACB at the plasma membrane and enhance penetration success of *Bgh* into barley
121 epidermal cells when overexpressed (41-43). In contrast, two other RACB protein-protein
122 interaction partners support resistance to fungal penetration. MICROTUBULE-ASSOCIATED
123 GTPASE ACTIVATING PROTEIN 1 (MAGAP1) enhances resistance towards *Bgh* and likely
124 regulates RACB by supporting GTP hydrolysis (34). Barley RBK1 interacts with CA-RACB in
125 yeast and *in planta*, and CA-RACB increases RBK1 kinase activity *in vitro*. RBK1 may be a
126 RACB effector kinase, since co-expression of CA-RACB and RBK1 results in co-localization
127 of both proteins at the plant plasma membrane via recruitment of the otherwise cytosolic RBK1.
128 However, opposite to the effect for RACB, transient knockdown of RBK1 results in increased
129 disease susceptibility and reduced microtubule stability (44). Another protein-protein
130 interaction partner of RBK1, S-PHASE KINASE 1-ASSOCIATED PROTEIN-LIKE (SKP1L), is
131 also involved in resistance towards *Bgh* (45). SKP1L may be a subunit of an SCF E3 ubiquitin
132 ligase complex, which targets specific proteins for polyubiquitination and proteasomal
133 degradation (19). In line with this predicted function, it was demonstrated that RBK1, SKP1L
134 and the 26S proteasome negatively influence protein abundance of CA-RACB, presumably
135 acting in a negative feedback-loop towards the ROP (45).

136 In this study, we confirm that kinase activity of RBK1 is strongly enhanced in the presence of
137 CA-RACB. This results in phosphorylation of both RBK1 and CA-RACB *in vitro*. Phosphosite
138 mapping revealed novel phosphorylated residues in RACB that were not previously described
139 to be modified in other RHO family proteins. We further found that CA-RACB shows an

140 ubiquitination-typical appearance of high molecular weight derivatives after proteasome
141 inhibition. Mass spectrometry revealed that CA-RACB is ubiquitinated in barley at K167, a
142 residue which is conserved in mammalian Rac1, Rac3 and all other ROPs of barley, rice and
143 Arabidopsis.

144

145 # Results

146 ## CA-RACB is phosphorylated by RBK1 *in vitro*

147 In a previous study, we showed that constitutively activated (CA-) RACB interacts with RBK1
148 *in vivo* and enhances its kinase activity *in vitro* (44). To test, if RACB is phosphorylated during
149 this protein-protein interaction, we carried out an *in vitro* radiolabeling kinase assay with
150 recombinant His-tagged RBK1 and CA-RACB (Fig 1A). For His-tagged *Medicago sativa*
151 MsROP6, Dorjgotov, Jurca (46) showed that RBK1-like RLCK VI_A kinases phosphorylate the
152 His-tag and linker, but not the ROP protein itself *in vitro*. We hence designed the cloning
153 strategy in a way that avoids creation of potential artificial phosphorylation sites, which could
154 otherwise be formed. Since RBK1 shows some constitutive kinase activity *in vitro* (44), we
155 used low RBK1 protein amounts in this assay. RBK1 alone displayed only weak
156 autophosphorylation activity under these conditions. In the presence of CA-RACB, we then
157 observed strong phosphorylation of both CA-RACB and RBK1. No phosphorylation could be
158 detected after incubation with a RBK1 kinase-dead mutant (KD, K245D, also see Fig 1B for
159 RBK1 protein stability) or in a water-control reaction.

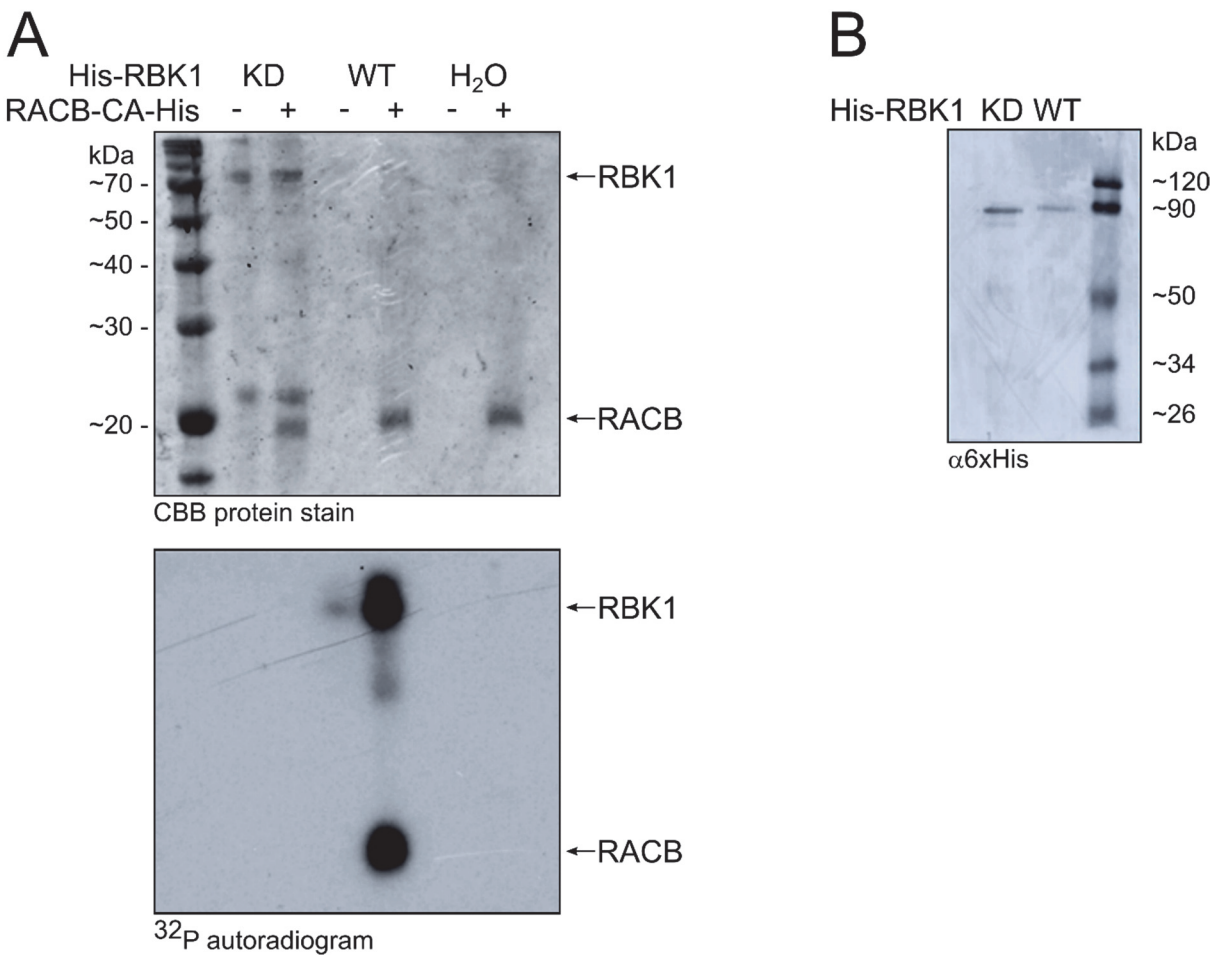

Fig 1. *In vitro* co-incubation of RACB and RBK1 results in phosphorylation of both proteins.

(A) Low amounts of His-tagged RBK1 alone show weak autophosphorylation *in vitro*. Kinase activity is enhanced by the presence of constitutively activated His-tagged CA-RACB, resulting in extensive phosphorylation of both proteins. Upper panel = protein loading control. Lower panel = autoradiogram showing ^{32}P-labelled, phosphorylated proteins. WT = wildtype RBK1; KD = kinase-dead RBK1 loss-of-function mutant (K245D); H_2O = no kinase control. Estimations of molecular weight are depicted in kilo Dalton (kDa) on the left.

(B) Western blot showing stability of both WT and KD His-RBK1.

To identify phosphosites in RACB, we conducted the *in vitro* kinase assay using unlabeled ATP and detected *in vitro* phosphosites of CA-RACB via mass spectrometry (Fig 2A). This

revealed high confidence CA-RACB peptides with phosphorylated residues at positions S97, T139, S159, S160 and T162. Since in the case of the neighboring serines S159 and S160 the localization of the phospho-modification could not be specifically assigned within the peptide sequence (S1 Table), both residues were treated as possible but alternative phosphosites. Using computational modelling of the RACB protein structure based on the protein models of GDP-bound AtROP4 and GTP-analog-bound HsRAC1, we suggest that S97, T139 and T162 are surface-exposed in RACB, whereas this is less clear for S159 and S160 (Fig 2B).

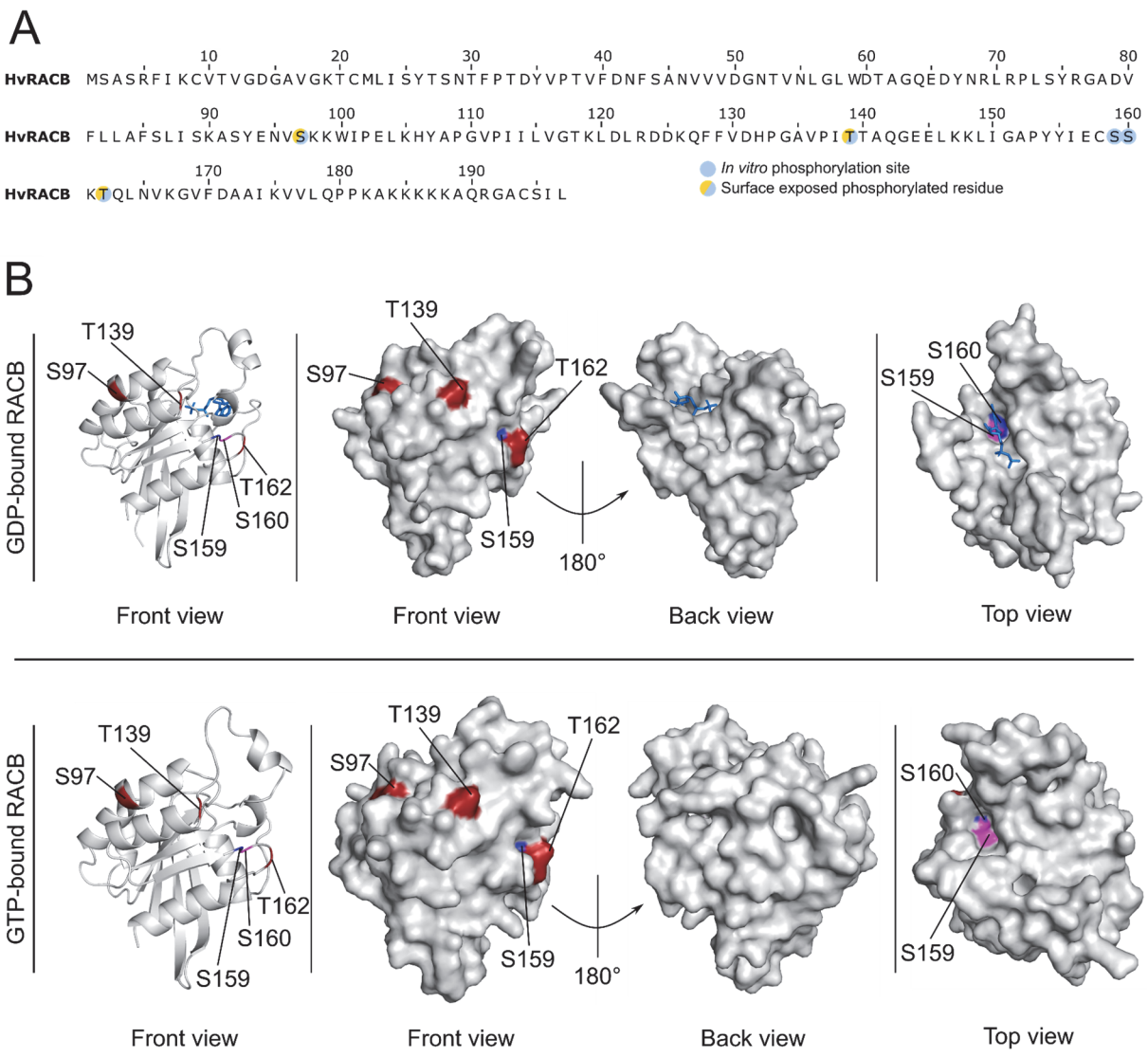

Fig 2. Surface-exposure of CA-RACB *in vitro* phosphosites.

182 **(A)** Phosphorylation sites of CA-RACB are shown in blue, predicted surface-exposed residues
183 are additionally highlighted in yellow. *In vitro* phosphorylation sites of RACB were identified by
184 mass spectrometry after *in vitro* co-incubation of CA-RACB and RBK1.

185 **(B)** Upper panel: the model of GDP-bound WT RACB (amino acids 1-178 from 197 total) was
186 built with GDP-bound AtROP4 as template (PDB entry: 2NTY.1 (47)). Lower panel: GTP-
187 bound WT RACB (amino acids 7-178 from 197 total) was modelled using HsRAC1 associated
188 with GNP (phosphoaminophosphonic acid-guanylate ester, a non-hydrolysable GTP-analog)
189 as template (PDB entry: 3TH5.1 (48)). Phosphorylated surface-exposed residues are shown
190 in red, GDP as ligand in blue. Only S97, T139 and T162 are surface-exposed, S159 (pink) and
191 S160 (blue) are not clearly exposed to the surface. Putative RACB folds were assembled by
192 homology-modelling using SWISS-MODEL (49). Surface structure (front, back and top view)
193 and cartoon (front view) illustrations were modelled in PyMOL (50).

194

195 We also tried to map *in vivo* phosphorylation sites for RACB. To this end, we made use of
196 transgenic barley lines overexpressing HA-tagged full-length CA-RACB, a cytosolic
197 non prenylated CA-RACB-ΔCSIL mutant (37) or the HA-tag alone. Initially, we generated 47
198 transgenic plants for HA-CA-RACB, 37 plants for HA-RACB-ΔCSIL and 40 plants for HA alone.
199 We propagated these lines and selected the offspring using PCR, resistance against
200 hygromycin and Western blotting (not shown). Thereby, we could see that all positive plants
201 expressed the expected HA-tagged proteins, except for the free HA-tag, which could not be
202 detected on a Western blot, most likely because the peptide is too small (Fig 3A). We further
203 analyzed three transgenic plants of one line per construct with regard to susceptibility towards
204 powdery mildew. Upon infection with *Bgh*, plants overexpressing full-length CA-RACB
205 displayed increased disease susceptibility compared to the free HA-control, whereas the
206 CA-RACB-ΔCSIL mutants did not show an altered disease phenotype (Fig 3B).

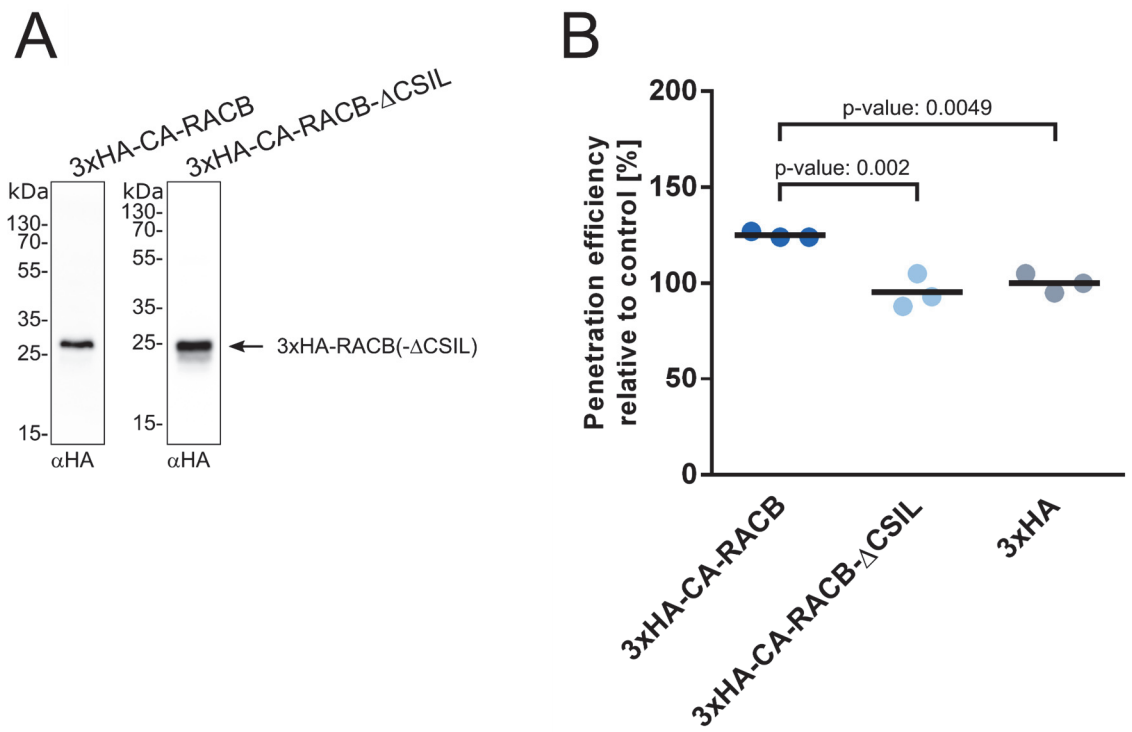

207

208 **Fig 3. Transgenic barley plants overexpressing HA-tagged CA-RACB show increased**
209 ***Bgh* susceptibility.**

210 **(A)** Both HA-tagged full-length CA-RACB and CA-RACB-ΔCSIL are stably expressed in
211 transgenic barley. Eluate fractions of anti-HA immunoprecipitations were analyzed by anti-HA
212 Western blotting. Plant material belonged to pools of transgenic lines BG657 E3 and E4 for
213 HA-CA-RACB and BG658 E4 and E9 HA-CA-RACB-ΔCSIL.

214 **(B)** Transgenic plants expressing full-length HA-tagged CA-RACB are more susceptible
215 towards penetration by *Bgh*, while plants expressing the truncated CA-RACB-ΔCSIL mutant
216 show the same level of susceptibility as the HA-control. For each construct, three plants of one
217 transgenic line were tested. Lines were BG657 E4 for 3x*HA*-CA-*RACB*, BG658 E4 for 3x*HA*-
218 CA-*RACB*-ΔCSIL and BG659 E2 for 3x*HA*. Each datapoint corresponds to one plant. Statistical
219 significances were determined using a One-way ANOVA with Tukey's HSD.

220

221 From the transgenic HA-CA-RACB overexpressing plants, we initially isolated protoplasts and
222 treated them with the proteasome inhibitor MG132 before protein extraction. We enriched

223 HA-tagged CA-RACB using immunoprecipitation, digested proteins with trypsin and selected
224 for phosphorylated peptides using Immobilized Metal Affinity Chromatography (IMAC).
225 Peptides and posttranslational modifications were identified via mass spectrometry, but did not
226 indicate CA-RACB phosphosites (not shown). In the following experiment, we co-expressed
227 RBK1 in transgenic protoplasts before MG132 treatment, and selectively skipped
228 immunoprecipitation or IMAC (S2A Fig). However, we were repeatedly unsuccessful in
229 identifying *in vivo* phosphopeptides of RACB (S2 Table). In a third approach, we tried to map
230 RACB phosphorylation after transient co-expression of RBK1 and proteasome inhibition by
231 MG132 in transgenic HA-CA-RACB overexpressing barley protoplasts. From this, we extracted
232 proteins, performed a tryptic digest and enriched phosphopeptides via IMAC. These samples
233 were subsequently decomplexed by high pH reversed-phase fractionation to increase the
234 discovery rate of peptides during mass spectrometry. This identified more than 5,000
235 phosphopeptides from diverse barley proteins, including ROP signaling components such as
236 three different barley ROPGAPs, thus providing a resource for the barley research community.
237 Because our experimental design included *in vivo* expression of combined or single GFP-
238 tagged RBK1 and HA-CA-RACB (S2B Fig), some of the mapped barley phosphosites might
239 be CA-RACB- and/or RBK1-dependent (S3 Table). Therefore, this needs further analysis.
240 Despite the high amount of identified phosphopeptides, no *in vivo* phosphopeptides of
241 CA-RACB were recovered.

242 Although we primarily aimed at identifying phosphopeptides of RACB, our datasets were
243 equally suitable for mapping phosphosites in RBK1 (Fig 4). In the *in vitro* kinase assay, we
244 found RBK1 to be phosphorylated at positions S26, S30, S98, S100, S107, T110, S155, T170
245 and S436. In the two experiments involving *in vivo* co-overexpression of CA-RACB and RBK1
246 (S2A Fig and Fig 4B), we found RBK1 phosphosites at positions S26, S30, S160, T170, S189,
247 S197, S518, T521 and S26, S30, S100, S107, S113, S114, S216, T525, respectively.
248 Overlapping sites from *in vitro* and at least one *in vivo* experiment are therefore S26, S30,
249 S100, S107 and T170.

A

B

In vitro sites	*In vivo* sites experiment 1	*In vivo* sites experiment 2
S26	S26	S26
S30	S30	S30
S98	-	-
S100	-	S100
S107	-	S107
T110	-	-
-	-	S113
-	-	S114
S155	-	-
-	S160	-
T170	T170	-
-	S189	-
-	S197	-
-	-	S216
S436	-	-
-	S518	-
-	S521	-
-	-	T525

Fig 4. Comparison between *in vitro* and *in vivo* RBK1 phosphosites.

(A) Barley RBK1 sequence with marked *in vitro* (blue) and *in vivo* (red) phosphosites. Residues phosphorylated under both conditions are shown in half circles of blue and red. *In vitro* phosphorylated amino acids were identified in an *in vitro* kinase assay, in which His-tagged RBK1 and His-tagged CA-RACB were co-incubated. *In vivo* phosphosites were found in transgenic HA-CA-RACB overexpressing protoplasts in the presence of transiently co-expressed GFP-tagged RBK1 and the proteasome-inhibitor MG132. Phosphopeptides were enriched from total protein extracts of protoplast lysates using IMAC (experiment 1) and additionally decomplexed by high pH reversed-phase fractionation (experiment 2). All *in vitro* and *in vivo* phosphosites were identified by mass spectrometry.

262 **(B)** List of RBK1 phosphosites from all *in vitro* and *in vivo* experiments.

263 CA-RACB is ubiquitinated *in vivo*

264 Previously, we found that the protein abundance of CA-RACB is negatively influenced by
265 RBK1, SKP1L and the proteasome (45). For this reason, we investigated if we could detect
266 ubiquitination of CA-RACB *in vivo*. We used MG132 for proteasome inhibition in primary leaves
267 of transgenic barley overexpressing HA-tagged CA-RACB. This led to detection of HA-CA-
268 RACB and higher molecular weight derivatives on Western blots after
269 αHA-immunoprecipitation and detection via anti-HA antibodies (Fig 5A). As this laddering is a
270 potential indicator for ubiquitination of a target protein (51, 52), we attempted to map the
271 residue(s) at which RACB might be ubiquitinated. We first conducted a global mass
272 spectrometry analysis, in which we specifically looked for branched amino acid sequences as
273 derived from ubiquitinated lysine residues after tryptic digest (S2C Fig). Interestingly, we found
274 the peptide containing RACB K167 carrying a mass shift equal to 2 glycine molecules (Fig 5B).
275 This mass shift indicates that K167 is indeed ubiquitinated, as two glycine residues typically
276 remain at ubiquitinated lysine residues (glyglycylation), whereas the rest of the ubiquitin moiety
277 is cleaved by trypsin during sample digestion (53). Evidence for RACB ubiquitination was
278 subsequently substantiated in a targeted parallel reaction monitoring (PRM) approach.
279 Comparison with other ROPs from barley, rice and Arabidopsis showed that RACB K167 is a
280 highly conserved residue in ROPs (Fig 6 and S3 Fig).

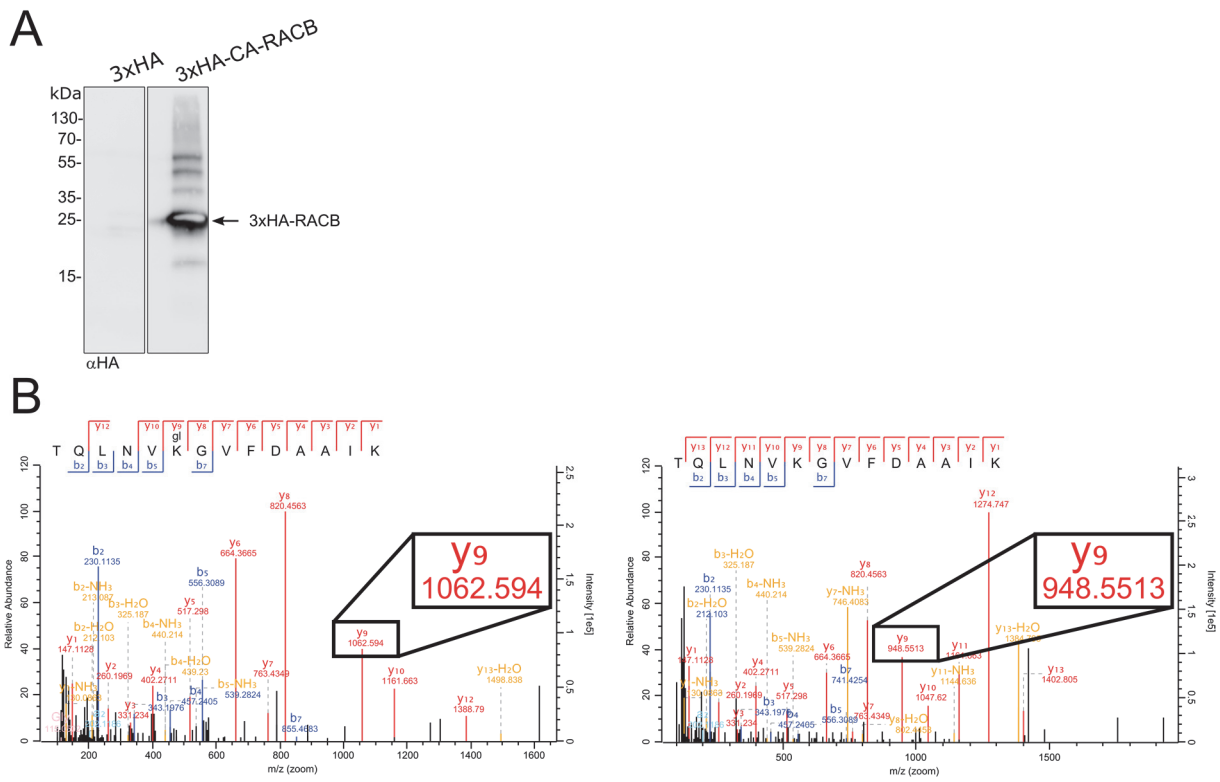

Fig 5. Constitutively activated RACB is ubiquitinated *in vivo*.

(A) HA-tagged CA-RACB and higher molecular weight bands were detected in an αHA-Western blot after MG132 treatment and αHA-immunoprecipitation from whole barley leaves stably expressing 3xHA or 3xHA-CA-RACB (Fig S2B). Plant material was pooled from transgenic lines BG657 E3 and E4 for 3xHA-CA-RACB and BG659 E2 and E3 for 3xHA.

(B) Ubiquitination of CA-RACB at K167 was identified by mass spectrometry in a workflow described in S2B Fig. The left graph shows spectra of the recovered ubiquitinated peptide, while the right graph shows the corresponding unmodified peptide. The black box illustrates one example: fragment "y9" was recovered with two different masses. The difference corresponds to that of 2 glycines, which is typical after a tryptic digest of ubiquitinated proteins (53). Example: $y9_{modified}$ (1062.59 m/z) – $y9_{unmodified}$ (948.55 m/z) = 114.04 m/z = 2 * glycine (57.02 m/z).

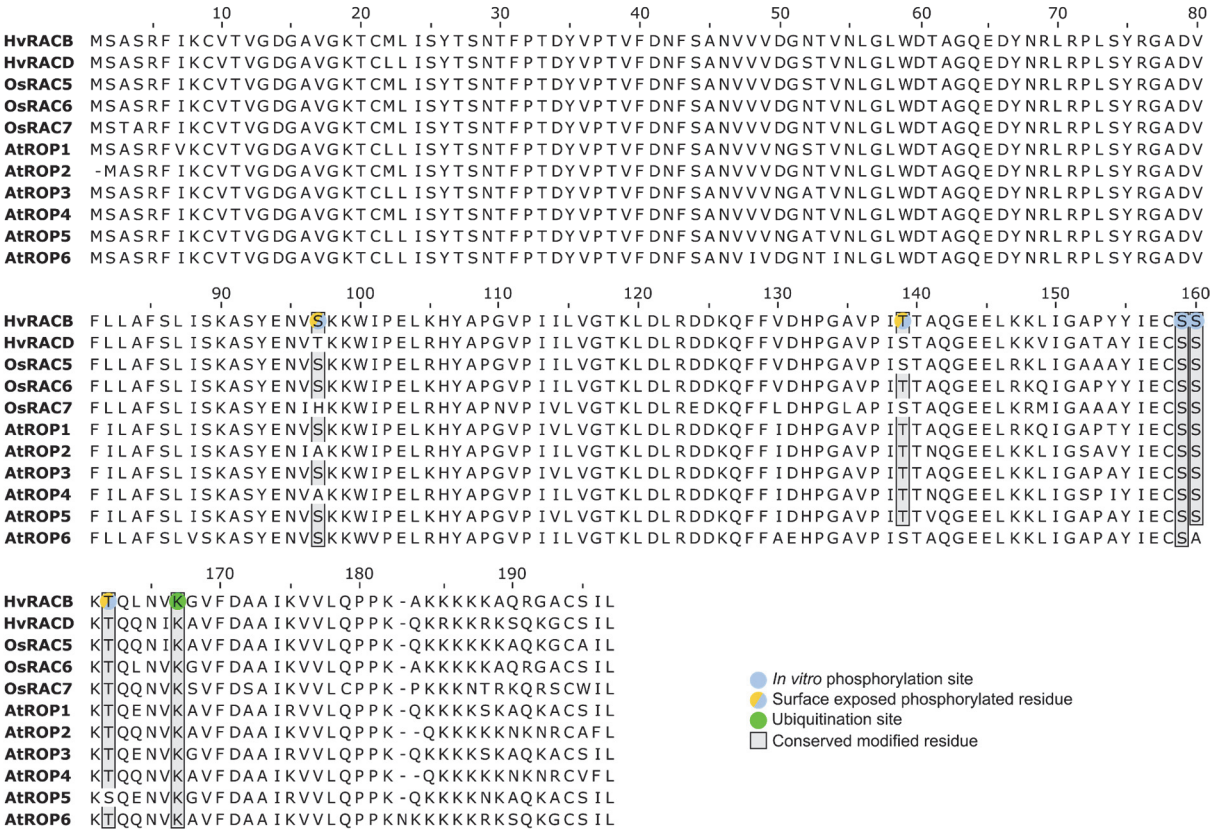

Fig 6. Alignment of type I ROPs from barley (*Hordeum vulgare*, *Hv*), rice (*Oryza sativa, Os*) and *Arabidopsis thaliana* (*At*). The ubiquitinated residue from CA-RACB (K167, green) is conserved across all type I ROPs from the three species (shaded box). *In vitro* phosphosites of RACB (blue) are conserved among some type I ROPs (shaded box). Surface-exposed phosphosites are additionally highlighted in yellow.

Discussion

Small RHO family proteins are signaling hubs and master regulators of cell polarity. Their function is tightly regulated, for instance by PTMs. Lipid modifications, phosphorylation and ubiquitination have been well described in the recent years, which can have an activity-enhancing or suppressing influence on the RHO protein, depending on each individual case. Other PTMs, such as glycosylation and adenylylation have been described, but they are predominantly employed by pathogens which target RHO family proteins via virulence effectors (54, 55).

312 In plants, ROP regulation by GEFs and GAPs has been shown (1, 34, 56-58), but there is little
313 data available on posttranslational regulation of ROPs beyond prenylation and *S*-acylation. In
314 this study, we show *in vitro* phosphorylation and *in vivo* ubiquitination of the barley ROP RACB.
315 S97, T139 and T162 *in vitro* phosphosites are predicted to be surface-exposed and therefore
316 could be also targets for RBK1-dependent phosphorylation of RACB *in vivo* (Fig 2). This is less
317 clear for S159 and S160. Nevertheless, one can speculate that they could become accessible
318 *in vivo* after other posttranslational modification of RACB, which cause a conformational shift
319 in the RACB structure. It would be furthermore possible that phosphorylation of S159/S160
320 interferes with RACB signaling, since these residues are in direct proximity of the putative
321 *S*-acylation site C158 and the nucleotide binding pocket (Fig 2 and S1 Fig; (59, 60)). However,
322 this remains hypothetical, as we did not find evidence for *in vivo* phosphorylation of these
323 amino acids. All five phosphorylated residues are partially conserved in other type I and type II
324 ROPs, indicating that these sites might be common targets for phosphorylation of RBK1-like
325 RLCK VI_A kinases in plants. The only known *in vivo* ROP phosphosite, S138 from AtROP10
326 and AtROP11 (S3 Fig; (32)), is not conserved in RACB, which indicates that this might be a
327 type II ROP-specific modification site. In any case, introducing point mutations at these sites
328 could help answering, which role they play in regulating ROP function.

329 Comparison of RACB phosphosites with those of mammalian Rac1 and RhoA revealed that
330 there is no overlap between mapped animal and plant phosphosites, although several modified
331 residues are conserved across kingdoms (S1 Fig). Thus, it is well possible that RACB is also
332 phosphorylated at Y67, S74 and S89 by other kinases, but in our *in vitro* and *in vivo*
333 approaches we did not identify modification of these residues. Still, conservation of these
334 amino acids suggests that RACB could be regulated in a similar fashion as mammalian RHO
335 family proteins. Interestingly, phosphorylation of these residues in mammalian RHO proteins
336 directly and indirectly regulates actin cytoskeleton dynamics (15, 18, 24), a process also
337 influenced by RACB in barley (38). Therefore, it remains conceivable that phosphorylation of
338 these conserved sites may be important for ROP regulation during plant cytoskeleton
339 rearrangement.

340 Using transgenic CA-RACB overexpressing plants, we were able to evidence RACB and
341 higher molecular weight derivatives on a Western blot after proteasome inhibition, which was
342 not observed in the absence of the proteasome inhibitor (compare Figs 3 and 5). Since these
343 higher molecular weight derivatives strongly resembled a typical ubiquitination pattern as
344 described for e.g. the plant pattern-recognition receptor flagellin sensing 2 (FLS2) (51, 52), we
345 excised these bands and investigated RACB ubiquitination via mass spectrometry. This way,
346 we identified RACB K167 as an ubiquitin acceptor site, which is fully conserved across all
347 ROPs of barley, rice and Arabidopsis (Fig 6 and S3 Fig). The respective residue is also
348 ubiquitinated in mammalian Rac1 and Rac3 by the SCF^{FBXL19}-complex, which leads to
349 proteasomal degradation of both proteins (18, 61). It remains to be elucidated, if comparable
350 regulatory mechanisms are conserved between RHO family proteins across kingdoms.

351 Two other ubiquitination sites present in mammalian RHO proteins are conserved in RACB
352 (S1 Fig): K8 and K148. Similar to phosphorylation, ubiquitination of the corresponding sites in
353 RhoA and Rac1 also influences actin cytoskeleton dynamics and associated cellular
354 processes, such as cell motility (20-22, 29, 62). Cross-kingdom conservation of these sites
355 raises the possibility that they might also be important for the regulation of RACB signaling,
356 but it is not yet known under which conditions these modifications might occur.

357 We previously hypothesized that RACB is regulated similarly to mammalian Rac1.
358 Phosphorylation of Rac1 S71 by AKT leads to SCF^{FBXL19}-mediated ubiquitination at Rac1 K166
359 and subsequent proteasomal degradation, which blocks Rac1 from signaling (Kwon et al.,
360 2000; Chang et al., 2011; Zhao et al., 2013). In plants, activated RACB would be
361 phosphorylated by RBK1 and then targeted for ubiquitination and degradation by an
362 SCF-complex containing SKP1L (44, 45). While we did find ubiquitination at RACB K167
363 (which corresponds to Rac1 K166, S1 Fig), we did not identify RACB S74 as a phosphorylation
364 site. One potential reason for this might be that RBK1 belongs to RLCK class VI_A (44, 63,
365 64), while AKT belongs to the AGC kinases (65). Interestingly, ROPs and AGCs also work
366 together in polar cell development: one AGCVIII kinase, D6PK, binds to specific membrane

367 lipids and cooperates with AtROP2/AtROP6 to form root hairs (66). Thus far, phosphorylation
368 of ROPs during interaction with AGC kinases has not been described. Hence, it is possible
369 that AGC kinases phosphorylate ROPs, with S74 being one of the potential targets. It could
370 also be that RACB S74 is not the target for a barley SKP1L-containing SCF-complex as
371 hypothesized above. One of the *in vitro* phosphosites in RACB could be alternatively
372 recognized and fulfill this role instead.

373 In Arabidopsis and barley, ROPs and RBK1 or related RLCK VI_A-class kinases seem to have
374 partially opposing biological functions. In previous studies, we have shown that HvRBK1 had
375 the opposite disease phenotype of RACB and negatively regulated its protein stability (44, 45).
376 In Arabidopsis, the ROP-activated RBK1-homolog RLCK VI_A3 is also involved in pathogen
377 resistance rather than susceptibility (63). In Arabidopsis, an auxin-responsive MPK-cascade
378 was associated with AtRBK1 (RLCK VI_A4) and ROP signaling. Enders and co-workers could
379 show that *mitogen-activated protein kinase kinase kinase 3* (*mkk3), mpk1* and *rbk1* knock-out
380 plants displayed hypersensitivity towards auxin, while *atrop4* and *atrop6* mutants were
381 defective in auxin sensing. Furthermore, they demonstrated that AtROP4 and AtROP6 might
382 be direct phosphorylation targets of AtRBK1 and hypothesized that AtRBK1-mediated
383 phosphorylation negatively influences the activity of both ROPs (31). However, this remains to
384 be fully shown, since phosphorylation of His-tagged AtROP4 and AtROP6 was investigated *in*
385 *vitro* and no phosphosites were mapped in this study. Nevertheless, this suggests a general
386 mechanism, in which ROPs are negatively regulated by phosphorylation through RLCK VI_A
387 members in distinct signaling branches.

388 Our data further support that posttranslational lipidation may be important for the signaling
389 ability of RACB. Only full-length CA-RACB increased barley susceptibility towards *Bgh*, while
390 the truncated CA-RACB-ΔCSIL mutant did not (Fig 3B). We have shown before that removal
391 of the CaaX-box prenylation motif from RACB results in a shift of CA-RACB's subcellular
392 localization from the plasma membrane to the cytosol and to loss of function in susceptibility
393 (37). Importance of the CaaX-box prenylation motif CSIL for RACB function is now confirmed

394 here with stable transgenic plants. We have also reported that the interaction of RACB with its
395 downstream effectors mostly takes place at the plant plasma membrane (34, 42, 43). It would
396 be interesting to see, if barley ROP effectors can still interact with CA-RACB-ΔCSIL *in planta*
397 and localize to the plasma membrane in presence of excessive amounts of cytosolic CA-
398 RACB-ΔCSIL. This could provide another piece of evidence that ROPs need to be plasma
399 membrane-localized to perform their function in signaling and to bind to downstream
400 interactors, as it has been described before (9, 10).

401 Conclusion

402 Regulation of RHO family proteins by PTMs has long been established in the animal research
403 field. In plants, however, we are only at the beginning of discovering these regulatory
404 mechanisms of PTMs in ROP signaling. Here, we present the first piece of data on *in vivo*
405 ubiquitination of one ROP from barley. The identified ubiquitination site is conserved in all
406 ROPs from barley, rice and Arabidopsis, and has been described before for mammalian
407 RACB-homologs. This suggests that the lysine residue corresponding to RACB K167 might be
408 a general target for ubiquitination across kingdoms. However, it remains to be elucidated, if
409 the function of this modification is also conserved in plants.

410 Experimental procedures

411 Heterologous protein expression, purification, and kinase activity
412 measurements

413 A cDNA clone of CA-*RACB* ((37), NCBI GenBank identifier for wildtype RACB: CAC83043.2)
414 was cloned into the bacterial expression vector pET26b out of frame of the N-terminal pelB,
415 but in frame with a C-terminal 6xHIS (Novagen, Merck KGaA, Darmstadt, Germany). This way,
416 no potential artificial phosphorylation site was included (46). The barley protein *RBK1* (NCBI
417 GenBank identifier: HE611049.1) was cloned into the pET28a vector in frame with an N-

418 terminal 6xHIS. Cloning was achieved by restriction-ligation after PCR amplification of the
419 cDNA inserts using *Eco*RI and *Xho*I flanking restriction sites on the C- and N-terminal
420 sequence-specific primers. CA-*RACB* was amplified using RACBCA-EcoRI-F +
421 RACBCA-XhoI-R primers, while both wildtype and kinase-dead *RBK1* were amplified with
422 RBK1-F + RBK1-R primers. The kinase dead (KD, K245D) mutant of *RBK1* was constructed
423 by PCR-mediated site-directed mutagenesis using primers RBK1KD-mut-F + RBK1KD-mut-R.
424 After PCR, the parental DNA was digested with *Dpn*I and the whole reaction was transformed
425 into *E. coli* DH5α cells. Following transformation, plasmids were extracted using a routine
426 Miniprep protocol and checked for mutation by sequencing. All primers can be found in S4
427 Table.

428 Proteins were purified using HisSelect Sepharose beads (Sigma-Aldrich, St. Louis, USA) and
429 the *in vitro* kinase reactions were carried out as described earlier (44, 45). Two parallel
430 reactions, one with and one without radioactive γ-^{32}P-ATP were performed with both WT and
431 KD RBK1, using the same amount of RACB-6xHIS as substrate. The amount of the proteins
432 in the reactions was app. 150 pmol of RACB-6xHIS with 4 pmol of 6xHis-RBK1-WT or 12 pmol
433 6xHis-RBK1-KD. The radioactive reaction for autoradiography contained 10 μM of cold ATP
434 and 0.2 MBq γ-^{32}P-ATP, while 100 μM ATP were included in the non-radioactive reaction
435 destined for mass spectrometry analysis. The reactions were terminated after 2.5 h and
436 proteins were separated on 12% SDS-polyacrylamide gels that were stained by Coomassie
437 Brilliant Blue using standard methods. Radioactive gels were dried and exposed to x-ray films.
438 From the non-radioactive gel, the band containing RACB-6xHIS was cut out and sent for
439 phosphosite mapping.

440 To show stability of both WT and KD 6xHis-RBK1, a Western blot was performed according to
441 standard procedures. His-tagged proteins were detected with an anti-polyHistidine−peroxidase
442 antibody (Sigma-Aldrich, St. Louis, USA, A7058).

443 Bioinformatical analysis

444 The putative RACB protein fold was built by homology-modelling using SWISS-MODEL (49)
445 with AtROP4 (PDB entry: 2NTY.1) as template. The final RACB model contained amino acids
446 1-178 (from 197 total amino acids). PyMOL V2.3.5 (50) was used to generate protein surface
447 structure and cartoon illustrations.

448 All protein sequence alignments were done in Jalview V2.11.0 (67) with the MAFFT algorithm
449 running at default settings (68). NCBI GenBank identifiers for all aligned proteins are:

450 HvRACB: CAC83043.2; HvRACD: CAD27895.1; HvRAC1: CAD57743.1; HvRAC3:
451 BAJ98596.1; HvROP4: CAD27896.1; HvROP6: CAD27894.1; OsRAC1: XP_015621645.1;
452 OsRAC2: XP_015638759.1; OsRAC3: XP_015625155.1; OsRAC4: XP_015641323.1;
453 OsRAC5: XP_015627011.1; OsRAC6: XP_015625732.1; OsRAC7: XP_015627590.1;
454 AtROP1: NP_190698.1; AtROP2: NP_173437.1; AtROP3: NP_001077910.1; AtROP4:
455 NP_177712.1; AtROP5: NP_195320.1; AtROP6: NP_001190916.1; AtROP9: NP_194624.1;
456 AtROP10: NP_566897.1; AtROP11: NP_201093.1; HsRAC1: NP_001003274.1; HsRHOA:
457 5FR2_A.

458 Generation of transgenic plants

459 A full-length cDNA clone of CA-*RACB* (carrying the G15V mutation as described in (37)) and
460 CA-*RACB*-ΔCSIL (lacking the last 4 amino acids, but with an artificial stop codon) were
461 amplified by PCR using primers RACBCA-Esp-Start + RACBCA-Esp-Stop and RACBCA-Esp-
462 Start + RACBCA-ΔCSIL-Esp-Stop, respectively. Both constructs were cloned first into
463 pGGEntL-EP12 and subsequently into pGGInAE-226n_35SP_Ntag-3xHA_35ST vectors using
464 procedures adapted from Golden Gate-based cloning (69), generating the 3x*HA*-CA-*RACB*(-
465 ΔCSIL) fusion constructs. From these vectors, the CA-*RACB*(-ΔCSIL) fusion constructs were
466 re-amplified by PCR using primers 3xHA-XmaI-F and RACBCA-XmaI-R (3x*HA*-CA-*RACB*) and
467 3xHA-XmaI-F + RACBCA-ΔCSIL-XmaI-R (3x*HA*-CA-*RACB*-ΔCSIL). The free 3x*HA*-control
468 was amplified using primers 3xHA-XmaI-F + UL1-XmaI-R. All constructs were introduced into
469 pUbifull-AB-M, a derivative of pNOS-AB-M (DNA-Cloning-Service, Hamburg, Germany) with

470 the maize *POLYUBIQUITIN 1* promoter being inserted in the multiple cloning site, by
471 restriction-ligation using *Xma*I. From there, *Sfi*I fragments were transferred into the generic
472 binary vector p6i-2x35S-TE9 (DNA-Cloning-Service, Hamburg, Germany). The binary
473 plasmids were transferred into *A. tumefaciens* strain AGL1 (70) and transgenic plants were
474 generated by agro-inoculation of immature barley embryos according to Hensel, Kastner (71).
475 Transgenic plants were identified by *HYGROMYCIN PHOSPHOTRANSFERASE*-specific
476 PCR, which yielded 47 lines for 3xHA-CA-RACB (BG657 E1-E49; E7 and E41 were not
477 transgenic), 37 lines for 3xHA-CA-RACB-ΔCSIL (BG658 E1-E39; E19 and E38 were not
478 transgenic) and 40 lines for 3xHA (BG659 E1-E42; E17 and E37 were not transgenic). All lines
479 were propagated under normal growth conditions in the greenhouse. Since all descending
480 lines are segregating in generation T_1, individual plants were screened for transgene
481 integration. This was achieved using Western blotting detecting the HA-tag (antibody: Anti-HA-
482 Peroxidase, Sigma-Aldrich, St. Louis, USA, 12013819001) and resistance against hygromycin-
483 induced discoloration. For the latter, 7 d old leaves were detached and placed on 0.8% water-
484 agar plates containing 200 µg/ml Hygromycin B (Roth, Karlsruhe, Germany, CP12.2). These
485 plates were put into growth chambers operating under long-day conditions (see below) for
486 roughly 4 d, until discoloration of hygromycin non-resistant plants was observed. After
487 screening, ten positive plants of two lines per construct were picked for an additional round of
488 propagation: we chose BG657 E3 and E4 for 3x*HA*-CA-*RACB*, BG658 E4 and E9 for 3x*HA*-
489 CA-*RACB*-ΔCSIL and BG659 E2 and E3 for 3x*HA*. Since the offspring of these lines remained
490 segregating in generation T_2 and no homozygous plants were obtained, all descendants were
491 screened for transgene expression as described above before use in any experiment. All
492 primers can be found in S4 Table.

493 Plant and fungal growth conditions

494 Transgenic barley (*Hordeum vulgare*) plants of spring-type cultivar Golden Promise were
495 grown under long-day conditions (16 h light, 8 h darkness) with a photon flux of at least 150
496 µmol m^{-2} s^{-1} at 18 °C and a relative humidity of 65%. Transgene-expressing plants of

497 generation T_2 were used in all experiments but one. An exception was made for the *Bgh*
498 penetration assay (see below), because propagation of the T_2 plants was not ready at that
499 time. Therefore, we used corresponding T_1 plants in this experiment. For all other experiments,
500 pools of T_2 plants expressing the same construct were used. For 3x*HA*-CA-*RACB*, we pooled
501 plants of lines BG657 E3 and E4, BG658 E4 and E9 for 3x*HA*-CA-*RACB*-ΔCSIL and BG659
502 E2 and E3 for 3x*HA*. The barley powdery mildew fungus *Blumeria graminis* f.sp. *hordei* race
503 A6 (*Bgh*) was propagated on non-transformed wildtype barley Golden Promise plants under
504 the same growth conditions.

505 Assessment of *Bgh* penetration efficiency

506 Primary leaves of transgenic plants were cut and placed on 0.8% water-agar plates. These
507 plates were inoculated with 100-130 spores/mm^2 of *Bgh* and placed under normal growth
508 conditions for 48 h, followed by fixing and destaining leaves in 70% (v/v) ethanol. Fungal
509 spores and appressoria were stained with an ink solution (10% (v/v) Pelikan Ink 4001®
510 (Pelikan, Hannover, Germany), 25% (v/v) acetic acid) and analysed by transmission light
511 microscopy. Haustorium establishment was counted as successful penetration, while stopped
512 fungal growth after appressorium formation was counted as successful plant defense. For each
513 construct, three transgene-expressing plants of one T_1 line (BG657 E4 for 3x*HA*-CA-*RACB*,
514 BG658 E4 for 3x*HA*-CA-*RACB*-ΔCSIL and BG659 E2 for 3x*HA*) were analyzed, with at least
515 96 evaluated plant-fungus interaction sites per plant. Data were visualized with GraphPad
516 Prism version 6. Statistical analysis was performed in RStudio V1.2.5033 (source:
517 https://rstudio.com/) using R V3.6.3 (source: https://www.R-project.org). Normal distribution
518 and homogeneity of variance in the penetration assay dataset were confirmed with Shapiro-
519 Wilk's test and Levene's test, respectively. Significant differences of results were assessed
520 using a One-way ANOVA with Tukey's HSD.

521 Protoplast transformation, proteasome inhibition and protein
522 extraction

523 Transgenic barley protoplasts stably expressing 3xHA-CA-RACB (pools of lines BG657 E3
524 and E4) or 3xHA (pools of lines BG659 E2 and E3) were isolated and super-transformed as
525 described in Reiner, Hoefle (45), with the following deviations: transformation reactions were
526 scaled to 1 ml of protoplasts and overnight incubation was conducted in 1 ml buffer WI in single
527 cell culture tubes. For transformation, 50 µg/ reaction of a plasmid coding for *GFP-RBK1* (from
528 Huesmann, Reiner (44)) or water (as a mock control) were used. Ten reactions per
529 combination (S2A and S2B Figs) were prepared. After overnight incubation, MG132 was
530 added to a final concentration of 10 µM, followed by incubation in the dark for 3 h. Protoplasts
531 of corresponding reactions were pooled and pelleted by centrifugation at 120 g. Supernatants
532 were removed and protoplasts were lysed by brief vortexing and snap-freezing in liquid
533 nitrogen. Proteins were resuspended in a modified extraction buffer (10% (w/v) glycerol, 25
534 mM Tris pH 7.5, 150 mM NaCl, 10 mM DTT, 1 mM PMSF, 1% sodium deoxycholate, 1x
535 protease inhibitor (Sigma-Aldrich, St. Louis, USA, P9599), 1 tablet /10 ml PhosSTOP™
536 (Sigma-Aldrich, St. Louis, USA, 4906845001)) and incubated on ice for 30 min with occasional
537 mixing. This solution was centrifuged at 4 °C to pellet cell debris, the supernatant was digested
538 with trypsin and used in phosphopeptide enrichment (S2A Fig (center panel) and S3B Fig). In
539 one experiment, where the phosphopeptide enrichment was skipped (S2A Fig (bottom panel)),
540 proteins were subjected to immunoprecipitation (see below), loaded on a SDS-PAGE and then
541 submitted to in-gel tryptic digest prior to mass spectrometry. All buffers described in the
542 immunoprecipitation paragraph were used. In another experiment (S2A Fig (top panel)),
543 protoplast lysates were subjected to immunoprecipitation using a modified extraction buffer
544 (10% (w/v) glycerol, 25 mM Tris pH 7.5, 150 mM NaCl, 10 mM DTT, 1 mM PMSF, 50 µM
545 MG132, 1x protease inhibitor (Sigma-Aldrich, St. Louis, USA, P9599), 1 tablet /10 ml
546 PhosSTOP™ (Sigma-Aldrich, St. Louis, USA, 4906845001)) and washing buffer (10% (w/v)
547 glycerol, 25 mM Tris pH 7.5, 150 mM NaCl, 1 mM PMSF, 50 µM MG132, 1x protease inhibitor
548 (Sigma-Aldrich, St. Louis, USA, P9599), 1 tablet /10 ml PhosSTOP™ (Sigma-Aldrich, St.
549 Louis, USA, 4906845001)) and used for on-bead tryptic digest prior to phosphopeptide
550 enrichment via IMAC.

551 ## Immunoprecipitation and Western blotting

552 In order to show protein stability of 3x*HA*-CA-*RACB* and 3x*HA*-CA-*RACB*-ΔCSIL, we
553 performed a routine HA-immunoprecipitation from untreated transgenic leaves (lines BG657
554 E3 and E4 and BG658 E4 and E9, respectively), followed by an anti-HA Western blot (see
555 below). For ubiquitination analysis, transgenic barley leaves expressing 3xHA-CA-RACB (lines
556 BG657 E3 and E4) or 3xHA (lines BG659 E2 and E3) were vacuum infiltrated for 3 min at -26
557 mm in Hg with a leaf-floating solution (0.45 M mannitol, 10 mM MES pH 5.7, 10 mM $CaCl_2$,
558 0.0316 g /10 ml Gamborg B5 medium including vitamins (Duchefa, RV Haarlem, The
559 Netherlands, G0210), 50 µM MG132). After incubation in the dark for 3 h, leaves were snap-
560 frozen in liquid nitrogen and homogenized using a TissueLyser II (QIAGEN, Hilden, Germany).
561 Proteins were resuspended in extraction buffer (10% (w/v) glycerol, 25 mM Tris pH 7.5, 1 mM
562 EDTA, 150 mM NaCl, 10 mM DTT, 1 mM PMSF, 0.5% Nonidet P40 substitute, 1x protease
563 inhibitor (Sigma-Aldrich, St. Louis, USA, P9599)) by tumbling end-over-end at 4 °C for 30 min.
564 Cell debris was removed by centrifugation and the supernatants were used for
565 immunoprecipitation (IP). IPs were conducted according to routine procedures. Briefly, for
566 each sample, 50 µM Pierce™ Anti-HA Magnetic Beads (Thermo Fisher Scientific, Waltham,
567 USA) were equilibrated 3x in extraction buffer before adding supernatants. HA-tagged proteins
568 were immunoprecipitated by tumbling end-over-end for 1 h at 4 °C, then washed 5x with
569 washing buffer (10% (w/v) glycerol, 25 mM Tris pH 7.5, 1 mM EDTA, 150 mM NaCl, 1 mM
570 PMSF, 1x protease inhibitor (Sigma-Aldrich, St. Louis, USA, P9599)). For selected RACB
571 phosphopeptide screenings (S2A Fig), the beads were directly prepared for mass
572 spectrometry. Otherwise, proteins were eluted in 100 µl of 2x NuPAGE™ LDS Sample Buffer
573 (Thermo Fisher Scientific, Waltham, USA, NP0008) and boiled at 95 °C for 10 min. After the
574 IP, 25 µl of eluate were separated on a 12% SDS-PAGE and proteins were transferred to a
575 PVDF membrane. HA-tagged proteins were detected with an Anti-HA-Peroxidase antibody
576 (Sigma-Aldrich, St. Louis, USA, 12013819001). For the RACB ubiquitination screening, the
577 remaining 75 µl were loaded on another 12% SDS-PAGE and silver stained after separation.

578 For this, the SDS-PAGE was incubated in a fixation solution (50% (v/v) methanol, 5% (v/v)
579 acetic acid, 45% (v/v) water) for 1 h and subsequently washed with water three times (two
580 times 2 min each, last time 1 h) on a shaking incubator. The gel was sensitized with a 0.02%
581 (w/v) sodium thiosulfate solution for 2 min, then briefly washed with water twice. Afterwards,
582 the gel was incubated at 4 °C in pre-chilled 0.1% (w/v) silver nitrate for 30 min, then rinsed two
583 times with water for 30 s each. In order to stain proteins, the gel was incubated in a developing
584 solution (0.04% (v/v) formaldehyde in 2% (w/v) sodium carbonate) until a sufficient degree of
585 staining had been obtained. Then, the gel was washed five times in 1% (v/v) acetic acid to stop
586 the reaction. Bands corresponding to 3xHA-CA-RACB and its higher molecular weight
587 derivatives were excised from the gel and the gel slices were prepared for mass spectrometry.
588 In order to show protein stability of 3x*HA*-CA-*RACB* and 3x*HA*-CA-*RACB*-ΔCSIL, we
589 performed a routine HA-immunoprecipitation from untreated transgenic leaves (lines BG657
590 E3 and E4 and BG658 E4 and E9, respectively), followed by an anti-HA Western blot.

591 Protein digest and phosphopeptide enrichment

592 In-gel digestion of SDS-PAGE gel segments was performed according to standard procedures.
593 Briefly, excised gel segments were reduced and alkylated with 10 mM dithiothreitol (DTT) and
594 55 mM chloroacetamide (CAA) followed by digestion with trypsin (Roche). Dried peptides were
595 reconstituted with 0.1% FA in water prior to LC-MS analysis. For peptide retention time
596 monitoring, PROCAL peptide standard (72) was added to peptide mixtures at a concentration
597 of 100 fmol on column.

598 On-bead digestion of one immunoprecipitation sample (from the experiment described in S2A
599 Fig (bottom panel)) was performed to facilitate a subsequent phosphopeptide enrichment. Dry
600 beads-bound proteins were incubated with urea buffer (8 M Urea, 50 mM Tris HCl pH 8.5, 10
601 mM DTT, cOmplete™ EDTA-free protease inhibitor cocktail (PIC) (Roche, Basel, Switzerland,
602 04693132001), Phosphatase inhibitor (PI-III; in-house, composition resembling Phosphatase
603 inhibitor cocktail 1 (P2850), 2 (P5726) and 3 (P0044) from Sigma-Aldrich, St. Louis, USA) for
604 one hour at 30 °C. The sample was alkylated (55 mM CAA), diluted 1:8 with digestion buffer

605 (50 mM Tris-HCl pH 8.5, 1 mM $CaCl_2$) and pre-digested with trypsin (1:100 protease:protein
606 ratio) for 4 hours followed by overnight digestion with trypsin (1:100 protease:protein ratio) at
607 37 °C. The sample was acidified to pH 3 with TFA and centrifuged at 14,000 *g* for 15 min at
608 4°C. The supernatant was desalted on a 50 mg SepPAC column (Waters, Milford, USA; elution
609 buffer 50% acetonitrile, 0.07% TFA).

610 Proteins from protoplast lysates were precipitated overnight with 10% trichloroacetic acid in
611 ice-cold acetone at -20°C. Precipitates were washed two times with ice-cold acetone and dry
612 samples re-suspended in urea buffer (8 M Urea, 50 mM Tris HCl pH 8.5, 1 mM DTT,
613 cOmpleteTM EDTA-free protease inhibitor cocktail (PIC) (Roche, Basel, Switzerland,
614 04693132001), Phosphatase inhibitor (PI-III; in-house, composition resembling Phosphatase
615 inhibitor cocktail 1 (P2850), 2 (P5726) and 3 (P0044) from Sigma-Aldrich, St. Louis, USA).

616 Protein concentration was determined with the Bradford assay (73). 200 µg (experiment
617 described in S2A Fig (center panel)) or 900 µg (all experiments described in S2B Fig) total
618 protein was reduced (10 mM DTT), alkylated (55 mM CAA), diluted 1:8 with digestion buffer
619 and pre-digested with trypsin (1:100 protease:protein ratio) for 4 hours followed by overnight
620 digestion with trypsin (1:100 protease:protein ratio) at 37 °C. Samples were acidified to pH 3
621 with TFA and centrifuged at 14,000 *g* for 15 min at 4 °C. Supernatants were desalted on 50 mg
622 SepPAC columns (Waters; elution buffer 50% acetonitrile, 0.07% TFA).

623 Phosphopeptide enrichment was performed using a Fe^{3+}-IMAC column (Propac IMAC-10 4x50
624 mm, Thermo Fisher Scientific, Waltham, USA) as described previously (74). Shortly, desalted
625 peptide samples were adjusted to 30% acetonitrile, 0.07% TFA. For quality control, 1.5 nmol
626 of a synthetic library of phosphopeptides and their corresponding non-phosphorylated
627 counterpart sequence (F1) (75), were spiked into samples prior to loading onto the column.
628 The enrichment was performed with buffer A (0.07% TFA, 30% acetonitrile) as wash buffer
629 and Buffer B (0.315% NH_4OH) as elution buffer. Collected full proteome and phosphopeptide
630 fractions were vacuum-dried and stored at -80°C until further use.

631 Phosphopeptides from the experiments described in S2A Fig (top and center panels) were re-
632 suspended in 50 mM citrate, 0.1% formic acid (FA) and desalted on self-packed StageTips
633 (five disks, Ø 1.5 mm C18 material, 3M Empore™, elution solvent 0.1% FA in 50% ACN).
634 Phosphopeptides from the experiment described in S2B Fig were re-suspended in 50 mM
635 citrate, 0.1% formic acid (FA), fractionated on basic reverse phase StageTip microcolumns
636 (five disks, Ø 1.5 mm C18 material, 3M Empore™) and pooled to 4 fractions, as described
637 previously (76). Dried peptides were reconstituted with 0.1% FA in water prior to LC-MS
638 analysis.

639 *In vitro* kinase assay samples were mixed 1:4 with urea buffer (8 M urea, 50 mM Tris-HCl pH
640 7.5). Samples were reduced (5 mM DTT, 1h, room temperature), alkylated (15 mM CAA, 30
641 min, room temperature) and subsequently diluted 1:8 with digestion buffer. In-solution pre-
642 digestion with trypsin (Roche, Basel, Switzerland) was performed for 4 hours at 37 °C (1:50
643 protease:protein ratio), followed by overnight digestion with trypsin (1:50 protease:protein
644 ratio). Samples were acidified to pH 3 using trifluoroacetic acid (TFA) and centrifuged at
645 14,000 *g* for 5 min. The supernatant was desalted on self-packed StageTips (four disks, Ø 1.5
646 mm C18 material, 3M Empore™, elution solvent 0.1% FA in 50% ACN). Dried peptides were
647 reconstituted with 0.1% FA in water prior to LC-MS analysis.

648 Mass spectrometry

649 Liquid chromatography-coupled mass spectrometry (LC-MS/MS) analysis was performed on
650 Orbitrap mass spectrometer systems (Thermo Fisher Scientific, Waltham, USA) coupled on-
651 line to a Dionex 3000 HPLC (Thermo Fisher Scientific, Waltham, USA). The liquid
652 chromatography setup consisted of a 75 µm × 2 cm trap column packed in-house with Reprosil
653 Pur ODS-3 5 µm particles (Dr. Maisch GmbH) and a 75 µm × 40 cm analytical column, packed
654 with 3 µm particles of C18 Reprosil Gold 120 (Dr. Maisch GmbH, Ammerbuch, Germany).
655 Peptides were loaded onto the trap column using 0.1% FA in water. Separation of the peptides
656 was performed by using a linear gradient from 4% to 32% ACN with 5% DMSO, 0.1% formic
657 acid in water over 60 min followed by a washing step (70 min total method length) at a flow

658 rate of 300 nl/min and a column temperature of 50 °C. For phosphopeptide fractions, the
659 gradient was adjusted to a two-step gradient from 4% to 27% ACN. The instruments were
660 operated in data-dependent mode, automatically switching between MS and MS2 scans.
661 For the RACB ubiquitination screen samples (S2C Fig), full-scan mass spectra (m/z 360-1300)
662 were acquired in profile mode on a Q Exactive HF with 60,000 resolution, an automatic gain
663 control (AGC) target value of 3e6 and 10 ms maximum injection time. For the top 20 precursor
664 ions, high resolution MS2 scans were performed using HCD fragmentation with 25%
665 normalized collision energy, 30,000 resolution, an AGC target value of 2e5, 50 ms maximum
666 injection time and 1.7 *m/z* isolation width in centroid mode. The underfill ratio was set to 1%
667 with a dynamic exclusion of 20 s. To confirm and more precisely monitor the GlyGly- and
668 phospho-modified peptides identified in the global analysis of these samples, a targeted
669 parallel reaction monitoring assay (PRM) was set up on the Q Exactive HF using the same LC
670 gradient settings. Peptide precursor charge states were chosen based on the previous
671 identification results. In addition, a selection of PROCAL retention time calibration mixture
672 peptides was monitored. PRM measurements were performed with the acquisition method
673 switching between experiments after one duty-cycle. The first experiment consisted of a full
674 scan MS1 spectrum recorded in the Orbitrap (360 to 1300 m/z, 15k resolution, AGC target
675 3e6, Maximum IT 50 ms). The second experiment consisted of a tMS2 PRM scan triggering
676 MS2 scans based on a list containing retention time window, m/z and charge information. For
677 the tMS2 PRM scan, the scheduled precursors were isolated (isolation window 1.3 m/z),
678 fragmented via HCD (NCE 25%) and recorded in the Orbitrap (120 to 2,000 m/z, 15k
679 resolution, AGC target 2e5, Maximum IT 100 ms).
680 For the kinase assay samples, full scan maximum injection time was 50 ms and MS2 scans
681 were performed with a resolution of 15,000 and 100 ms maximum injection time. His-tagged
682 CA-RACB and RBK1 peptides were set on an inclusion list and the dynamic exclusion set to
683 5s.
684 For the experiments described in S2B Fig, full-scan mass spectra (m/z 360-1300) were
685 acquired in profile mode on a Q Exactive HF-X with 60,000 resolution, an automatic gain

686 control (AGC) target value of 3e6 and 45 ms maximum injection time. For the top 20 precursor
687 ions, high resolution MS2 scans were performed using HCD fragmentation with 26 %
688 normalized collision energy, 30,000 resolution, an AGC target value of 2e5, and 1.3 *m/z*
689 isolation width in centroid mode. The intensity threshold was set to 2.2e4 with a dynamic
690 exclusion of 25 s. RACB and RBK1 peptides were set on an inclusion list. Full proteome
691 samples were measured with 50 ms maximum injection time for MS2 scans, phosphopeptide
692 samples with 100 ms.
693 For the experiment described in S2A Fig, full-scan mass spectra (m/z 360-1,300) were
694 acquired in profile mode on an Orbitrap Fusion LUMOS with 60,000 resolution, an automatic
695 gain control (AGC) target value of 4e5 and 50 ms maximum injection time. For the top 15
696 precursor ions, high resolution MS2 scans were performed using HCD fragmentation with 30%
697 normalized collision energy, 30,000 resolution, an AGC target value of 5e4, 120 ms maximum
698 injection time and 1.7 *m/z* isolation width in centroid mode. The intensity threshold was set to
699 2.5e4 with a dynamic exclusion of either 27 s (all peptides) or 10 s (RACB peptides set on an
700 inclusion list).
701 Peptide and protein identification and quantification was performed with MaxQuant (77) using
702 standard settings (version 1.5.8.3). Raw files were searched against a barley database
703 (160517_Hv_IBSC_PGSB_r1_proteins_HighConf_REPR_annotation.fasta; IPK Gatersleben)
704 and common contaminants. For the experiments described in S2B Fig, we added the
705 phosphopeptide library sequences (75). For the kinase assay dataset, we used the
706 recombinant protein sequences and an *E. coli* reference database (uniprot-
707 proteome_UP000000625). Carbamidomethylated cysteine was set as fixed modification and
708 oxidation of methionine, and N-terminal protein acetylation as variable modifications. Lysine
709 ubiquitylation, phosphorylation of serine, threonine or tyrosine were set as variable
710 modification were applicable. An m/z value of 115.0502 was specified as diagnostic ion for
711 lysine glyglycylation (78). Trypsin/P was specified as the proteolytic enzyme, with up to two
712 missed cleavage sites allowed. The match between run function was enabled for matching

samples and between fractions. Results were filtered to 1% PSM, protein and Site FDR. MS spectra were displayed with MaxQuant viewer.

RAW files from the PRM measurement of the ubiquitination screen samples were imported into Skyline (64-bit, v.4.1.0.11796) (79) for data filtering and analysis and transition selection was manually refined to include site determining ions for each modification site. Peaks were integrated using the automatic peak finding function followed by manual curation of all peak boundaries and transitions. The summed area under the fragment ion traces data for every transition was exported for data visualization in Microsoft Excel and used to confirm the expected relative quantity of modified RACB peptides based on the gel segment.

The mass spectrometry proteomics data have been deposited to the ProteomeXchange Consortium via the PRIDE (80) partner repository with the dataset identifier PXD019273.

Acknowledgements

We acknowledge the technical assistance of Cornelia Marthe (IPK Gatersleben) in generating the transgenic barley used in this study and Dalma Ménesi for her help with protein purifications (IPB, BRC Szeged). We are grateful to the TUM plant technology center for support in propagation of transgenic barley plants.

FUNDING

This work was supported by a research grant to R.H. from the German Research Foundation in frame of the collaborative research center SFB924. The contribution of A.F. was supported by a grant from the National Research, Development, and Innovation Office (#K101112; Hungary). The funders had no role in study design, data collection and analysis, decision to publish, or preparation of the manuscript.

References

1. Akamatsu A, Wong HL, Fujiwara M, Okuda J, Nishide K, Uno K, et al. An OsCEBiP/OsCERK1-OsRacGEF1-OsRac1 module is an essential early component of chitin-induced rice immunity. Cell host & microbe. 2013;13(4):465-76.
2. Ebine K, Fujimoto M, Okatani Y, Nishiyama T, Goh T, Ito E, et al. A membrane trafficking pathway regulated by the plant-specific RAB GTPase ARA6. Nat Cell Biol. 2011;13(7):853-9.
3. Irani K, Xia Y, Zweier JL, Sollott SJ, Der CJ, Fearon ER, et al. Mitogenic signaling mediated by oxidants in Ras-transformed fibroblasts. Science. 1997;275(5306):1649-52.
4. Jones MA, Shen J-J, Fu Y, Li H, Yang Z, Grierson CS. The Arabidopsis Rop2 GTPase is a positive regulator of both root hair initiation and tip growth. The Plant Cell. 2002;14(4):763-76.
5. Lin Y, Yang Z. Inhibition of Pollen Tube Elongation by Microinjected Anti-Rop1Ps Antibodies Suggests a Crucial Role for Rho-Type GTPases in the Control of Tip Growth. Plant Cell. 1997;9(9):1647-59.
6. Yang Z. Cell polarity signaling in Arabidopsis. Annu Rev Cell Dev Biol. 2008;24:551-75.
7. Wennerberg K, Rossman KL, Der CJ. The Ras superfamily at a glance. J Cell Sci. 2005;118(Pt 5):843-6.
8. Lawson CD, Ridley AJ. Rho GTPase signaling complexes in cell migration and invasion. J Cell Biol. 2018;217(2):447-57.
9. Sorek N, Gutman O, Bar E, Abu-Abied M, Feng X, Running MP, et al. Differential effects of prenylation and s-acylation on type I and II ROPS membrane interaction and function. Plant Physiol. 2011;155(2):706-20.
10. Yalovsky S. Protein lipid modifications and the regulation of ROP GTPase function. J Exp Bot. 2015;66(6):1617-24.
11. Berken A, Wittinghofer A. Structure and function of Rho-type molecular switches in plants. Plant Physiol Biochem. 2008;46(3):380-93.
12. Berken A. ROPs in the spotlight of plant signal transduction. Cell Mol Life Sci. 2006;63(21):2446-59.
13. Milburn MV, Tong L, deVos AM, Brunger A, Yamaizumi Z, Nishimura S, et al. Molecular switch for signal transduction: structural differences between active and inactive forms of protooncogenic ras proteins. Science. 1990;247(4945):939.
14. Boulter E, Garcia-Mata R. RhoGDI: A rheostat for the Rho switch. Small GTPases. 2010;1(1):65-8.
15. Chang F, Lemmon C, Lietha D, Eck M, Romer L. Tyrosine phosphorylation of Rac1: a role in regulation of cell spreading. PLoS One. 2011;6(12):e28587.
16. Tong J, Li L, Ballermann B, Wang Z. Phosphorylation of Rac1 T108 by extracellular signal-regulated kinase in response to epidermal growth factor: a novel mechanism to regulate Rac1 function. Mol Cell Biol. 2013;33(22):4538-51.
17. Kwon T, Chun J, Kim JH, Kang SS. Akt protein kinase inhibits Rac1-GTP binding through phosphorylation at serine 71 of Rac1. Journal of Biological Chemistry. 2000;275(1):423-8.
18. Zhao J, Mialki RK, Wei J, Coon TA, Zou C, Chen BB, et al. SCF E3 ligase F-box protein complex SCFFBXL19 regulates cell migration by mediating Rac1 ubiquitination and degradation. The FASEB Journal. 2013;27(7):2611-9.
19. Hua Z, Vierstra RD. The cullin-RING ubiquitin-protein ligases. Annu Rev Plant Biol. 2011;62:299-334.
20. Castillo-Lluva S, Tan CT, Daugaard M, Sorensen PH, Malliri A. The tumour suppressor HACE1 controls cell migration by regulating Rac1 degradation. Oncogene. 2013;32(13):1735-42.
21. Oberoi TK, Dogan T, Hocking JC, Scholz R-P, Mooz J, Anderson CL, et al. IAPs regulate the plasticity of cell migration by directly targeting Rac1 for degradation. EMBO J. 2012;31(1):14-28.

785 22. Torrino S, Visvikis O, Doye A, Boyer L, Stefani C, Munro P, et al. The E3 ubiquitin-ligase HACE1
786 catalyzes the ubiquitylation of active Rac1. Dev Cell. 2011;21(5):959-65.
787 23. Tang J, Ip JPK, Ye T, Ng Y-P, Yung W-H, Wu Z, et al. Cdk5-Dependent Mst3 Phosphorylation and
788 Activity Regulate Neuronal Migration through RhoA Inhibition. The Journal of Neuroscience.
789 2014;34(22):7425-36.
790 24. Tong J, Li L, Ballermann B, Wang Z. Phosphorylation and Activation of RhoA by ERK in Response
791 to Epidermal Growth Factor Stimulation. PLoS One. 2016;11(1):e0147103.
792 25. Ellerbroek SM, Wennerberg K, Burridge K. Serine phosphorylation negatively regulates RhoA
793 in vivo. The Journal of biological chemistry. 2003;278(21):19023-31.
794 26. Forget M-A, Desrosiers RR, Gingras D, Béliveau R. Phosphorylation states of Cdc42 and RhoA
795 regulate their interactions with Rho GDP dissociation inhibitor and their extraction from biological
796 membranes. Biochemical Journal. 2002;361(2):243-54.
797 27. Lang P, Gesbert F, Delespine-Carmagnat M, Stancou R, Pouchelet M, Bertoglio J. Protein kinase
798 A phosphorylation of RhoA mediates the morphological and functional effects of cyclic AMP in
799 cytotoxic lymphocytes. EMBO J. 1996;15(3):510-9.
800 28. Rolli-Derkinderen M, Sauzeau V, Boyer L, Lemichez E, Baron C, Henrion D, et al.
801 Phosphorylation of serine 188 protects RhoA from ubiquitin/proteasome-mediated degradation in
802 vascular smooth muscle cells. Circulation research. 2005;96(11):1152-60.
803 29. Ozdamar B, Bose R, Barrios-Rodiles M, Wang HR, Zhang Y, Wrana JL. Regulation of the polarity
804 protein Par6 by TGFbeta receptors controls epithelial cell plasticity. Science. 2005;307(5715):1603-9.
805 30. Wei J, Mialki RK, Dong S, Khoo A, Mallampalli RK, Zhao Y, et al. A new mechanism of RhoA
806 ubiquitination and degradation: roles of SCF(FBXL19) E3 ligase and Erk2. Biochimica et biophysica acta.
807 2013;1833(12):2757-64.
808 31. Enders TA, Frick EM, Strader LC. An Arabidopsis kinase cascade influences auxin-responsive
809 cell expansion. Plant J. 2017;92(1):68-81.
810 32. Mergner J, Frejno M, List M, Papacek M, Chen X, Chaudhary A, et al. Mass-spectrometry-based
811 draft of the Arabidopsis proteome. Nature. 2020.
812 33. Fodor-Dunai C, Fricke I, Potocky M, Dorjgotov D, Domoki M, Jurca ME, et al. The
813 phosphomimetic mutation of an evolutionarily conserved serine residue affects the signaling
814 properties of Rho of plants (ROPs). Plant J. 2011;66(4):669-79.
815 34. Hoefle C, Huesmann C, Schultheiss H, Börnke F, Hensel G, Kumlehn J, et al. A barley ROP
816 GTPase ACTIVATING PROTEIN associates with microtubules and regulates entry of the barley powdery
817 mildew fungus into leaf epidermal cells. The Plant Cell. 2011;23(6):2422-39.
818 35. Pathuri IP, Zellerhoff N, Schaffrath U, Hensel G, Kumlehn J, Kogel KH, et al. Constitutively
819 activated barley ROPs modulate epidermal cell size, defense reactions and interactions with fungal leaf
820 pathogens. Plant Cell Rep. 2008;27(12):1877-87.
821 36. Schultheiss H, Dechert C, Kogel K-H, Hückelhoven R. A small GTP-binding host protein is
822 required for entry of powdery mildew fungus into epidermal cells of barley. Plant Physiology.
823 2002;128(4):1447-54.
824 37. Schultheiss H, Dechert C, Kogel KH, Huckelhoven R. Functional analysis of barley RAC/ROP G-
825 protein family members in susceptibility to the powdery mildew fungus. Plant J. 2003;36(5):589-601.
826 38. Opalski KS, Schultheiss H, Kogel KH, Huckelhoven R. The receptor-like MLO protein and the
827 RAC/ROP family G-protein RACB modulate actin reorganization in barley attacked by the biotrophic
828 powdery mildew fungus Blumeria graminis f.sp. hordei. Plant J. 2005;41(2):291-303.
829 39. Pathuri IP, Imani J, Babaeizad V, Kogel K-H, Eichmann R, Hückelhoven R. Ectopic expression of
830 barley constitutively activated ROPs supports susceptibility to powdery mildew and bacterial wildfire
831 in tobacco. European journal of plant pathology. 2009;125(2):317-27.
832 40. Scheler B, Schnepf V, Galgenmuller C, Ranf S, Huckelhoven R. Barley disease susceptibility
833 factor RACB acts in epidermal cell polarity and positioning of the nucleus. J Exp Bot. 2016;67(11):3263-
834 75.
835 41. Engelhardt S, Kopischke M, Hofer J, Probst K, McCollum C, Hückelhoven R. Barley RIC157 is
836 involved in RACB-mediated susceptibility to powdery mildew. bioRxiv. 2019:848226.

42. McCollum C, Engelhardt S, Hückelhoven R. ROP INTERACTIVE PARTNER b interacts with the ROP GTPase RACB and supports fungal penetration into barley epidermal cells. bioRxiv. 2019:750265.
43. Schultheiss H, Preuss J, Pircher T, Eichmann R, Huckelhoven R. Barley RIC171 interacts with RACB in planta and supports entry of the powdery mildew fungus. Cell Microbiol. 2008;10(9):1815-26.
44. Huesmann C, Reiner T, Hoefle C, Preuss J, Jurca ME, Domoki M, et al. Barley ROP binding kinase1 is involved in microtubule organization and in basal penetration resistance to the barley powdery mildew fungus. Plant Physiol. 2012;159(1):311-20.
45. Reiner T, Hoefle C, Hückelhoven R. A barley SKP1-like protein controls abundance of the susceptibility factor RACB and influences the interaction of barley with the barley powdery mildew fungus. Molecular plant pathology. 2016;17(2):184-95.
46. Dorjgotov D, Jurca ME, Fodor-Dunai C, Szűcs A, Ötvös K, Klement É, et al. Plant Rho-type (Rop) GTPase-dependent activation of receptor-like cytoplasmic kinases in vitro. FEBS Letters. 2009;583(7):1175-82.
47. Thomas C, Fricke I, Scrima A, Berken A, Wittinghofer A. Structural evidence for a common intermediate in small G protein-GEF reactions. Mol Cell. 2007;25(1):141-9.
48. Krauthammer M, Kong Y, Ha BH, Evans P, Bacchiocchi A, McCusker JP, et al. Exome sequencing identifies recurrent somatic RAC1 mutations in melanoma. Nat Genet. 2012;44(9):1006-14.
49. Waterhouse A, Bertoni M, Bienert S, Studer G, Tauriello G, Gumienny R, et al. SWISS-MODEL: homology modelling of protein structures and complexes. Nucleic acids research. 2018;46(W1):W296-W303.
50. Schrodinger, LLC. The PyMOL Molecular Graphics System, Version 1.8. 2015.
51. Gohre V, Spallek T, Haweker H, Mersmann S, Mentzel T, Boller T, et al. Plant pattern-recognition receptor FLS2 is directed for degradation by the bacterial ubiquitin ligase AvrPtoB. Curr Biol. 2008;18(23):1824-32.
52. Lu D, Lin W, Gao X, Wu S, Cheng C, Avila J, et al. Direct ubiquitination of pattern recognition receptor FLS2 attenuates plant innate immunity. Science. 2011;332(6036):1439-42.
53. Peng J, Schwartz D, Elias JE, Thoreen CC, Cheng D, Marsischky G, et al. A proteomics approach to understanding protein ubiquitination. Nat Biotechnol. 2003;21(8):921-6.
54. Jank T, Bogdanović X, Wirth C, Haaf E, Spoerner M, Böhmer KE, et al. A bacterial toxin catalyzing tyrosine glycosylation of Rho and deamidation of Gq and Gi proteins. Nature Structural & Molecular Biology. 2013;20(11):1273-80.
55. Worby CA, Mattoo S, Kruger RP, Corbeil LB, Koller A, Mendez JC, et al. The fic domain: regulation of cell signaling by adenylylation. Mol Cell. 2009;34(1):93-103.
56. Berken A, Thomas C, Wittinghofer A. A new family of RhoGEFs activates the Rop molecular switch in plants. Nature. 2005;436(7054):1176-80.
57. Wu G, Li H, Yang Z. Arabidopsis RopGAPs Are a Novel Family of Rho GTPase-Activating Proteins that Require the Cdc42/Rac-Interactive Binding Motif for Rop-Specific GTPase Stimulation. Plant Physiology. 2000;124(4):1625-36.
58. Klahre U, Kost B. Tobacco RhoGTPase ACTIVATING PROTEIN1 Spatially Restricts Signaling of RAC/Rop to the Apex of Pollen Tubes. The Plant Cell. 2006;18(11):3033-46.
59. Sorek N, Poraty L, Sternberg H, Buriakovsky E, Bar E, Lewinsohn E, et al. Corrected and Republished from: Activation Status-Coupled Transient S-Acylation Determines Membrane Partitioning of a Plant Rho-Related GTPase. Molecular and Cellular Biology. 2017;37(23):e00333-17.
60. Sorek N, Segev O, Gutman O, Bar E, Richter S, Poraty L, et al. An S-Acylation Switch of Conserved G Domain Cysteines Is Required for Polarity Signaling by ROP GTPases. Current Biology. 2010;20(10):914-20.
61. Dong S, Zhao J, Wei J, Bowser RK, Khoo A, Liu Z, et al. F-box protein complex FBXL19 regulates TGFbeta1-induced E-cadherin down-regulation by mediating Rac3 ubiquitination and degradation. Mol Cancer. 2014;13(1):76.
62. Wang H-R, Zhang Y, Ozdamar B, Ogunjimi AA, Alexandrova E, Thomsen GH, et al. Regulation of Cell Polarity and Protrusion Formation by Targeting RhoA for Degradation. Science. 2003;302(5651):1775-9.

889 63. Reiner T, Hoefle C, Huesmann C, Ménesi D, Fehér A, Hückelhoven R. The Arabidopsis ROP-
890 activated receptor-like cytoplasmic kinase RLCK VI_A3 is involved in control of basal resistance to
891 powdery mildew and trichome branching. Plant Cell Reports. 2015;34(3):457-68.
892 64. Jurca ME, Bottka S, Fehér A. Characterization of a family of Arabidopsis receptor-like
893 cytoplasmic kinases (RLCK class VI). Plant Cell Reports. 2008;27(4):739-48.
894 65. Rademacher EH, Offringa R. Evolutionary Adaptations of Plant AGC Kinases: From Light
895 Signaling to Cell Polarity Regulation. Front Plant Sci. 2012;3:250.
896 66. Stanislas T, Huser A, Barbosa IC, Kiefer CS, Brackmann K, Pietra S, et al. Arabidopsis D6PK is a
897 lipid domain-dependent mediator of root epidermal planar polarity. Nat Plants. 2015;1(11):15162.
898 67. Waterhouse AM, Procter JB, Martin DM, Clamp M, Barton GJ. Jalview Version 2--a multiple
899 sequence alignment editor and analysis workbench. Bioinformatics. 2009;25(9):1189-91.
900 68. Katoh K, Toh H. Parallelization of the MAFFT multiple sequence alignment program.
901 Bioinformatics. 2010;26(15):1899-900.
902 69. Engler C, Kandzia R, Marillonnet S. A one pot, one step, precision cloning method with high
903 throughput capability. PLoS One. 2008;3(11):e3647.
904 70. Lazo GR, Stein PA, Ludwig RA. A DNA transformation-competent Arabidopsis genomic library
905 in Agrobacterium. Bio/technology (Nature Publishing Company). 1991;9(10):963-7.
906 71. Hensel G, Kastner C, Oleszczuk S, Riechen J, Kumlehn J. Agrobacterium-mediated gene transfer
907 to cereal crop plants: current protocols for barley, wheat, triticale, and maize. International journal of
908 plant genomics. 2009;2009:835608.
909 72. Zolg DP, Wilhelm M, Yu P, Knaute T, Zerweck J, Wenschuh H, et al. PROCAL: a set of 40 peptide
910 standards for retention time indexing, column performance monitoring, and collision energy
911 calibration. Proteomics. 2017;17(21):1700263.
912 73. Bradford MM. A rapid and sensitive method for the quantitation of microgram quantities of
913 protein utilizing the principle of protein-dye binding. Anal Biochem. 1976;72:248-54.
914 74. Ruprecht B, Koch H, Domasinska P, Frejno M, Kuster B, Lemeer S. Optimized Enrichment of
915 Phosphoproteomes by Fe-IMAC Column Chromatography. Methods Mol Biol. 2017;1550:47-60.
916 75. Marx H, Lemeer S, Schliep JE, Matheron L, Mohammed S, Cox J, et al. A large synthetic peptide
917 and phosphopeptide reference library for mass spectrometry–based proteomics. Nature
918 biotechnology. 2013;31(6):557-64.
919 76. Ruprecht B, Zecha J, Zolg DP, Kuster B. High pH Reversed-Phase Micro-Columns for Simple,
920 Sensitive, and Efficient Fractionation of Proteome and (TMT labeled) Phosphoproteome Digests.
921 Methods Mol Biol. 2017;1550:83-98.
922 77. Cox J, Mann M. MaxQuant enables high peptide identification rates, individualized ppb-range
923 mass accuracies and proteome-wide protein quantification. Nature biotechnology. 2008;26(12):1367-
924 72.
925 78. Zolg DP, Wilhelm M, Schmidt T, Medard G, Zerweck J, Knaute T, et al. ProteomeTools:
926 Systematic characterization of 21 post-translational protein modifications by liquid chromatography
927 tandem mass spectrometry (LC-MS/MS) using synthetic peptides. Molecular & Cellular Proteomics.
928 2018;17(9):1850-63.
929 79. MacLean B, Tomazela DM, Shulman N, Chambers M, Finney GL, Frewen B, et al. Skyline: an
930 open source document editor for creating and analyzing targeted proteomics experiments.
931 Bioinformatics. 2010;26(7):966-8.
932 80. Vizcaíno JA, Csordas A, Del-Toro N, Dianes JA, Griss J, Lavidas I, et al. 2016 update of the PRIDE
933 database and its related tools. Nucleic acids research. 2016;44(D1):D447-D56.

934

935

Supporting information

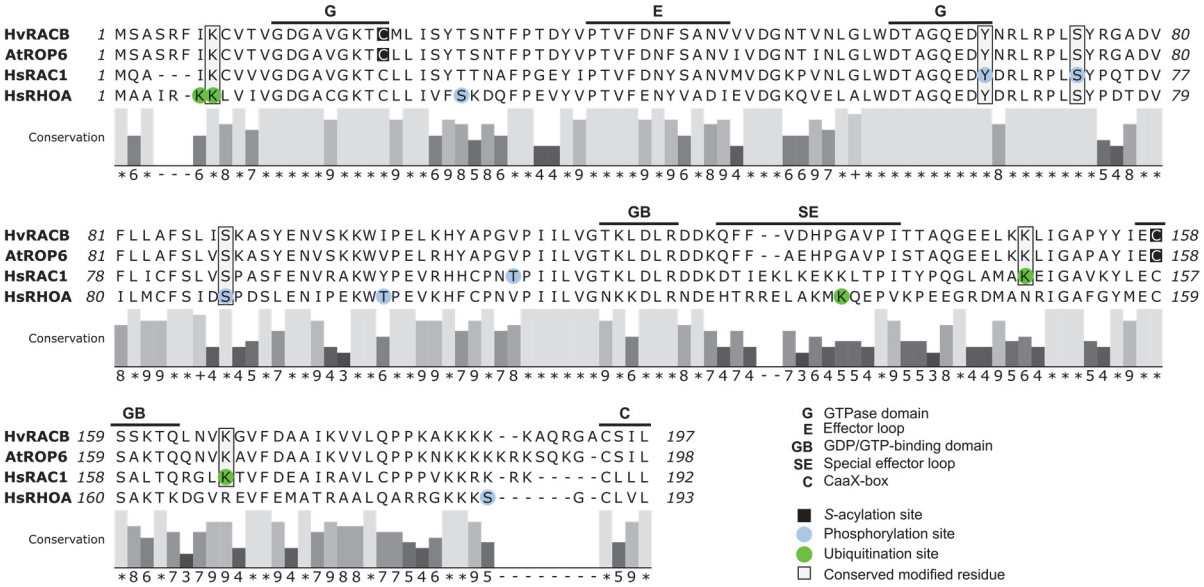

S1 Fig. Alignment of RACB with AtROP6, HsRAC1 and HsRHOA.

Previously published phosphorylation (blue) and ubiquitination (green) sites of mammalian Rac1 and RhoA are highlighted here in the human RAC1 and RHOA sequences. Conserved sites are highlighted in grey boxes. Additionally, the GTPase domain (G), effector loop (E), nucleotide-binding domain (GB), special effector loop (SE) and CaaX-box prenylation motif (C) are illustrated and were taken from Schultheiss, Dechert (37). AtROP6 has been shown to be transiently *S*-acylated at two cysteines (59, 60), which are also conserved in RACB (black boxes). Conservation of amino acids was determined using MAFFT multiple-sequence alignment in Jalview (67, 68). Conservation scores range from 0 to 11 and are shown as bars (dark grey = less conserved, light grey = highly conserved). Scores of 0, 10, and 11 are shown as “-“, “+” and “*”, respectively).

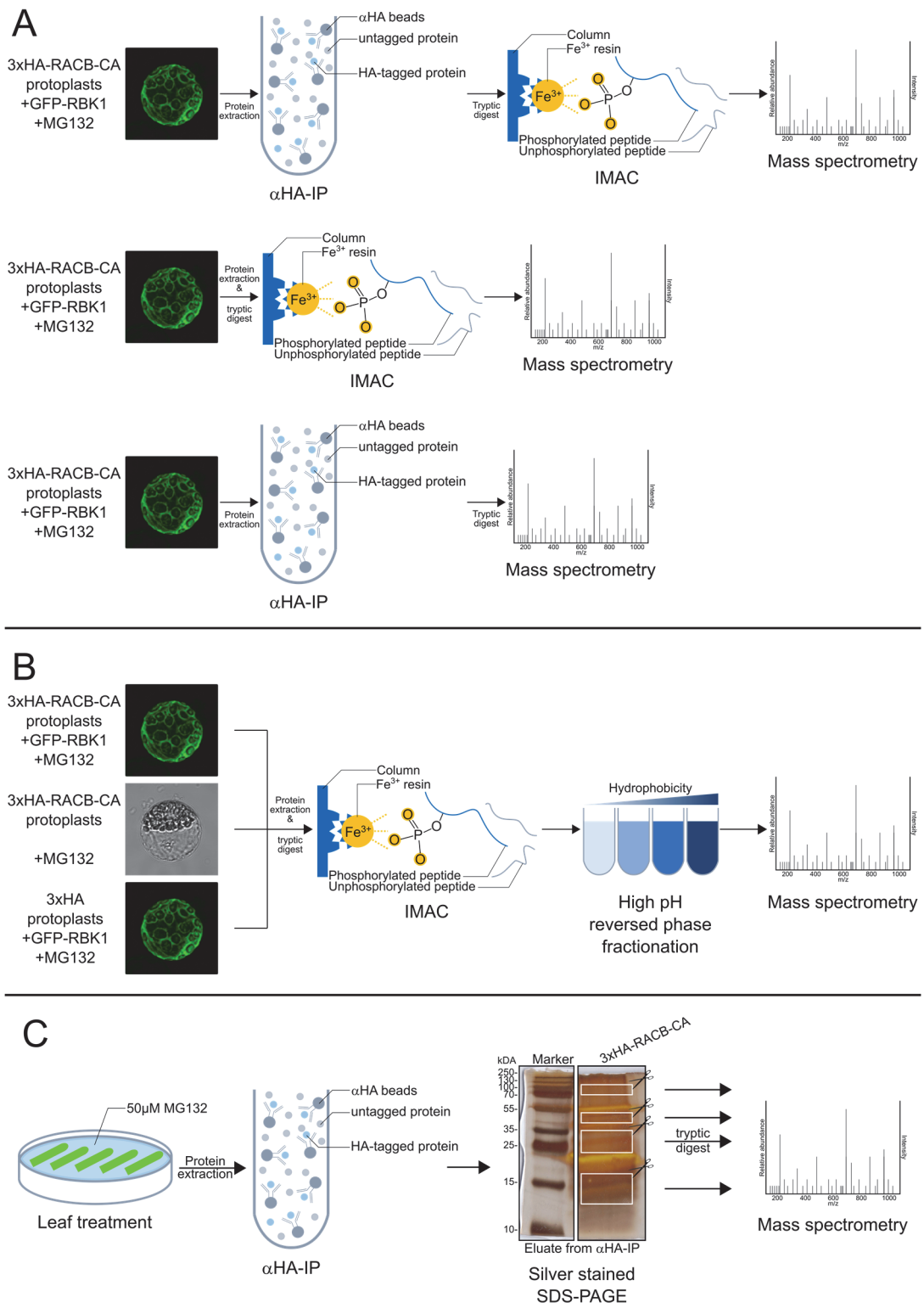

S2 Fig. Workflows designed to identify RACB phosphorylation and ubiquitination.

(A) Identification of phosphorylated peptides after CA-RACB and RBK1 overexpression. Protoplasts were isolated from stably-transgenic barley leaves overexpressing 3xHA-CA-

957 RACB (pooled lines BG657 E3 and E4). These protoplasts were transiently super-transformed
958 with GFP-RBK1 to stimulate phosphorylation events of proteins associated with the
959 RACB/RBK1 pathway. After transformation, all protoplasts were treated with MG132 and
960 proteins were extracted. HA-tagged proteins were first enriched using immunoprecipitation,
961 followed by tryptic digest and phosphopeptide enrichment via IMAC (top panel). In two cases,
962 immunoprecipitation or IMAC were skipped (center and lower panel, respectively).
963 Phosphorylated peptides were identified using mass spectrometry.

964 **(B)** Second experiment to identify phosphorylated peptides after CA-RACB and/or RBK1
965 overexpression. Protoplasts were isolated from stably transgenic barley leaves overexpressing
966 either 3xHA (lines BG659 E2 and E3) or 3xHA-CA-RACB (lines BG657 E3 and E4). These
967 protoplasts were super-transformed with GFP-RBK1. After transformation, all protoplasts
968 (including an untransformed 3xHA-CA-RACB control) were treated with MG132. Proteins were
969 extracted and digested with trypsin, followed by enrichment of phosphopeptides using IMAC.
970 These samples were decomplexed by fractionating the phosphorylated proteins according to
971 their hydrophobicity. Phosphorylated peptides were identified by mass spectrometry.

972 **(C)** Analysis of CA-RACB ubiquitination by a targeted approach. Transgenic barley leaves
973 overexpressing 3xHA-CA-RACB (from pooled lines BG657 E3 and E4) were floated on a
974 solution containing MG132. HA-containing proteins were enriched by immunoprecipitation and
975 loaded on a SDS-PAGE. Following silver-staining, RACB-containing bands and those
976 corresponding to the higher molecular weight derivatives shown in Fig 5A were excised from
977 the gel (white boxes). After solubilization and tryptic digest, modification of RACB-peptides
978 was investigated via mass spectrometry.

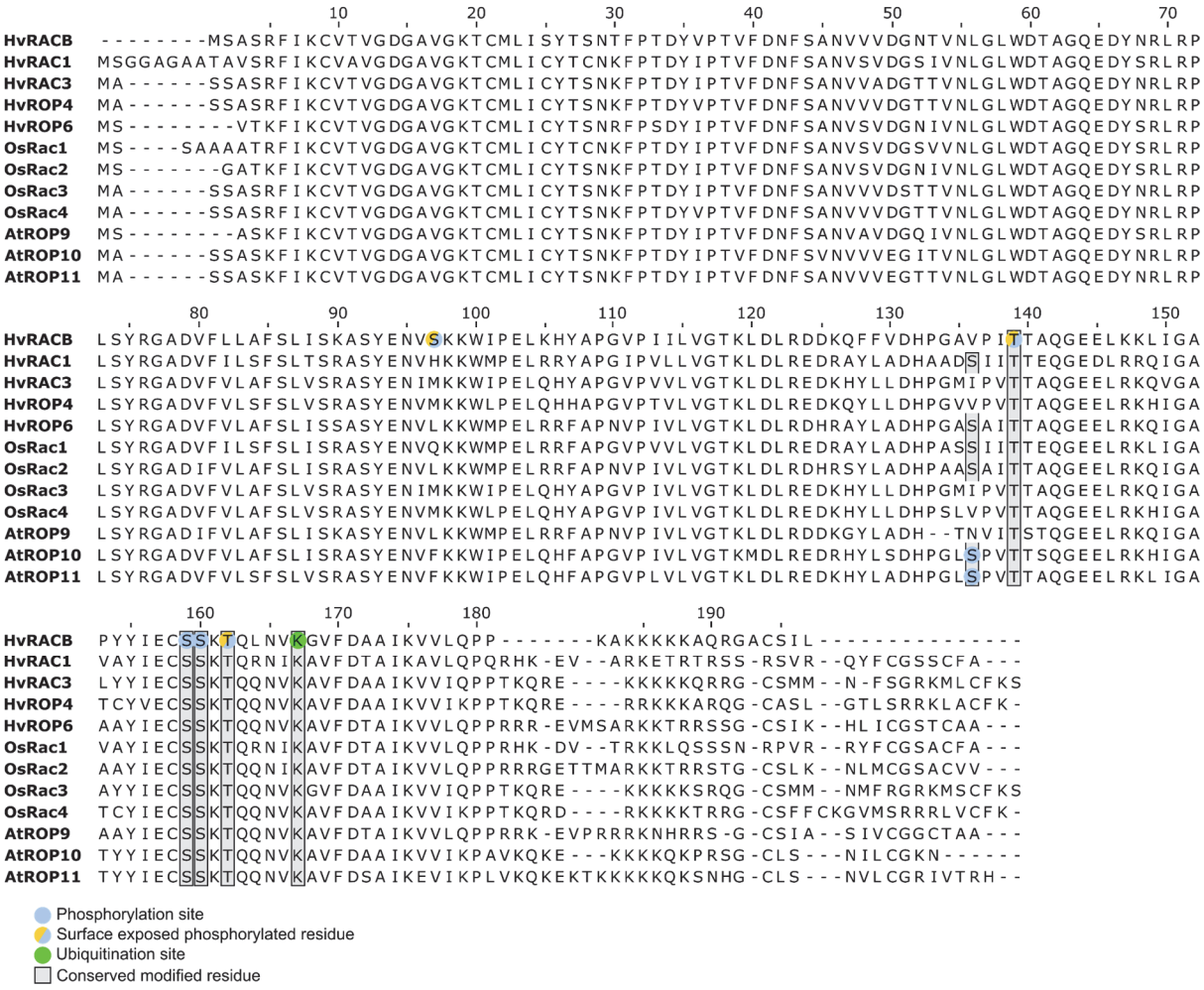

S3 Fig. Alignment of barley RACB with type II ROPs from barley, rice *Arabidopsis thaliana*.

The CA-RACB ubiquitination site at K167 (green) is conserved in all type II ROPs from the three species (shaded box). *In vitro* phosphorylation sites of RACB (blue) are conserved among most type II ROPs (shaded box). Surface-exposed phosphosites are additionally shown in yellow. Conserved of amino acids were identified and aligned using MAFFT multiple-sequence alignment in Jalview (67, 68).

988 **S1 Table. Dataset of the mass spectrometry analysis of the recombinant RACB and**
989 **RBK1 *in vitro* kinase assay.**

990 **S2 Table. Dataset of the first mass-spectrometry experiment to identify *in vivo***
991 **phosphorylation of CA-RACB.** This dataset contains all identified barley phosphopeptides
992 originating from transgenic HA-CA-RACB overexpressing protoplasts, which were transformed
993 with GFP-RBK1 and treated with MG132. HA-tagged proteins and/or phosphopeptides were
994 enriched by HA-immunoprecipitation and IMAC, respectively (S2A Fig). All peptides and their
995 modifications were identified by mass spectrometry. Of main interest are the gene identifiers
996 and peptides with phosphorylated residues and associated localization scores.

997 **S3 Table. Dataset of the second mass-spectrometry experiment to identify *in vivo***
998 **phosphorylation of CA-RACB.** Dataset comprising all recovered barley phosphopeptides
999 from protoplasts of stable transgenic barley plants. Phosphopeptides were enriched from
1000 full-protein extracts of either HA- or HA-CA-RACB overexpressing protoplasts, which were co-
1001 transformed with GFP-RBK1 and incubated with MG132. Samples were decomplexed by
1002 fractionating phosphopeptides according to their hydrophobicity (S2B Fig). All peptides and
1003 their modifications were identified by mass spectrometry. Non-enriched full-protein samples
1004 (FP) were included in mass spectrometry analyses, but did not yield many phosphopeptides.
1005 Of main interest in this dataset are the gene identifiers and peptides with phosphorylated amino
1006 acids and their corresponding localization scores.

1007 **S4 Table. List of all primers used in this study.**

1008